

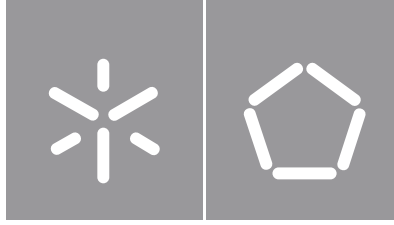


Tomás Ramos Ribeiro

**Production of melt-spun fibers with heat
conduction properties**

Universidade do Minho
Escola de Engenharia





Universidade do Minho

Escola de Engenharia

Tomás Ramos Ribeiro

**Production of melt-spun fibers with heat
conduction properties**

Dissertação de Mestrado

Mestrado Integrado em Engenharia de Polímeros

Trabalho realizado sob a orientação de:

Professora Doutora Maria Conceição Paiva

Mestre Sofia Silva

Direitos de Autor e Condições de Utilização do Trabalho por Terceiros

Este é um trabalho académico que pode ser utilizado por terceiros desde que respeitadas as regras e boas práticas internacionalmente aceites, no que concerne aos direitos de autor e direitos conexos.

Assim, o presente trabalho pode ser utilizado nos termos previstos na licença abaixo indicada.

Caso o utilizador necessite de permissão para poder fazer um uso do trabalho em condições não previstas no licenciamento indicado, deverá contactar o autor, através do RepositóriUM da Universidade do Minho.

Licença concedida aos utilizadores deste trabalho:



Atribuição-NãoComercial-Compartilha Igual

CC BY-NC-SA

<https://creativecommons.org/licenses/by-nc-sa/4.0/>

Acknowledgements

Throughout my life, I always had people beside me that helped me in every step of the way, and the development of this work was no exception. With that being said, I would like to thank everyone that, directly or indirectly, guided and supported me in the conclusion of this important stage of my life. My genuine thanks to everyone.

First and foremost, I would like to express my sincere gratitude to my parents, Helena, and Paulo, for the values and all the education they passed on to me and for their willingness to share their experiences and insights that help me become the person I am today. To my sister, Carolina, for the sense of responsibility and fraternity. And, by extension, to all my family.

I must thank my advisor, PhD professor Maria Conceição Paiva, for all the guidance, support, and outstanding feedback during my master's thesis work.

To CeNTI, for all the conditions provided and to all the Functional Fibers team for welcoming me and for all the help provided. A special thanks to Sofia and Cíntia for guiding me during the development of this work, for letting me learn from my mistakes and for the immense sharing of knowledge.

I would like to highlight my friend José who has offered me invaluable advices that will benefit me during my whole life and for making this journey much more enjoyable.

To my group of friends "Glassware", for the friendship and companionship during this last five years.

In addition, I would like to mention my group of friends "Não tejas medo" for always having my back and making me understand the real meaning of friendship.

Lastly, to my girlfriend Lara, for the love and unconditional support.

Without all of you this would not be possible. My deepest and sincere appreciation.

Statement of integrity

I hereby declare having conducted this academic work with integrity. I confirm that I have not used plagiarism or any form of undue use of information or falsification of results along the process leading to its elaboration.

I further declare that I have fully acknowledged the Code of Ethical Conduct of the University of Minho.

University of Minho, October 2023

Tomás Ramos Ribeiro

Resumo

O objetivo deste trabalho consiste na produção de fibras pela técnica *melt-spinning*, baseadas em nanocompósitos polímero/nanopartículas de carbono. com propriedades de condução de calor, através do Efeito de Joule. O motivo deste trabalho envolve dar o seguimento da produção de nanocompósitos condutores até às fibras multifilamento, que ainda é um tema pouco abordado.

Primeiramente, a preparação dos nanocompósitos foi dividida em duas etapas: (i) produção de compósitos com poli(butileno tereftalato) (PBT) e nanotubos de carbono de parede múltipla (MWCNTs) para determinação do limiar de percolação elétrica; (ii) produção de compósitos híbridos com MWCNTs e grafite, PBT/MWCNTs/G, para estudar o efeito da grafite na condutividade elétrica dos nanocompósitos. O limiar de percolação elétrico do compósito PBT/MWCNTs encontra-se abaixo de 1 %(m/m) de MWCNTs, observando-se um aumento da condutividade elétrica em 10 ordens de grandeza (de 1×10^{-15} para $2,11 \times 10^{-5}$ S/m). O valor máximo de condutividade elétrica foi 1,75 S/m no compósito com 5 %(m/m) de MWCNTs. A adição de grafite no composto PBT/MWCNTs selecionado (PBT/2%MWCNTs) teve um efeito negativo, reduzindo a condutividade elétrica entre 2 e 4 ordens de grandeza. Para estudar esta diminuição, a morfologia dos compósitos híbridos foi caracterizada para avaliar a presença de aglomerados. Por último, para selecionar o composto com melhor resposta térmica, os nanocompósitos PBT/MWCNTs com composição próxima do limiar de percolação (1, 2 e 3 %(m/m)) foram submetidos a testes de aquecimento para analisar a ocorrência do Efeito de Joule. Os resultados demonstraram melhor resposta térmica para o compósito PBT/3%MWCNTs, atingindo uma temperatura de 41,2 °C com uma tensão de 12 V.

A última etapa do trabalho consistiu na produção de multifilamentos pela técnica de *melt-spinning*. As propriedades elétricas, térmicas e mecânicas dos multifilamentos foram analisados. Foram obtidos multifilamentos com condutividade elétrica de $2,86 \times 10^{-4}$ S/m. No entanto, os ensaios mecânicos de tração indicaram que a adição dos MWCNTs na matriz de PBT reduziu a tenacidade e o alongamento à ruptura dos multifilamentos. Os testes de aquecimento demonstraram que o efeito de Joule não era significativo nos multifilamentos, pois a temperatura permaneceu inalterada (≈ 26 °C) mesmo com a aplicação de uma tensão de 48 V.

Palavras-chave: condutividade elétrica, Efeito de Joule, fibras multifilamento, *melt-spinning*

Abstract

The objective of this study was to produce melt-spinning fibers, based on nanocomposites polymer/carbon nanoparticles with heat conduction properties, by Joule effect. The development of this work was motivated since there are few researches involving heat conduction in melt-spun fibers.

Firstly, the nanocomposites preparation was carried in two steps: (i) production of composites with poly(butylene terephthalate) (PBT) and multi-walled carbon nanotubes (MWCNTs) and determination of the electrical percolation threshold; (ii) production of hybrid composites with MWCNTs and graphite, PBT/MWCNTs/G, to study the effect of graphite in the electrical conductivity of the nanocomposites. The electrical percolation threshold of the PBT/MWCNTs nanocomposites was reached below 1 wt.% with an increase of the electrical conductivity of 10 orders of magnitude (from 1×10^{-15} to $2,11 \times 10^{-5}$ S/m). The highest value of electrical conductivity was 1,75 S/m with a filler content of 5 wt.% of MWCNTs. The addition of graphite into the selected PBT/MWCNTs nanocomposite (PBT/2%MWCNTs) had a negative effect, decreasing the electrical conductivity between 2 and 4 orders of magnitude. To study this decrease, the hybrid nanocomposites morphology was characterized to evaluate the presence of agglomerates. Lastly, in order to select the nanocomposite with the best thermal response, the PBT/MWCNTs nanocomposites with a filler content near the electrical percolation threshold (1 wt.%, 2 wt.% and 3 wt.%) were submitted to heating tests to analyze the occurrence of the Joule Effect. The results showed better thermal response for the PBT/3%MWCNTs, reaching a temperature of 41,2 °C with a voltage of 12 V.

The last stage of this work consisted in the production of multifilament fibers using the melt-spinning technique. Afterwards, the produced fibers were characterized by their electrical, thermal, and mechanical properties. It was possible to produce multifilaments with an electrical conductivity of $2,86 \times 10^{-4}$ S/m. However, the mechanical tests of the multifilaments proved that the MWCNTs addition to the PBT matrix reduced the tenacity and elongation at break of the multifilaments. The heating tests showed that the Joule effect was not significant in the multifilaments, since the temperature remained stable (≈ 26 °C) even with an applied voltage of 48 V.

Keywords: electrical conductivity, Joule Effect, melt-spinning, multifilament fibers.

Content

I. Introduction	1
1. Background	1
2. Objectives and Work Planning	3
3. Dissertation Structure	4
II. Literature Review	5
4. State of art	5
4.1. Nanocomposites	6
4.2. Conductive fillers	6
4.3. Electrical conductivity in nanocomposites	7
4.4. Heat conduction in nanocomposites and multifilaments	11
4.5. Dispersion of carbon nanoparticles	12
4.6. Melt-spinning technique	13
4.7. Materials selection	16
4.7.1. Poly(butylene terephthalate)	16
4.7.2. Carbon nanotubes	17
4.7.3. Graphite	19
III. Materials and Methods	20
5. Materials	20
6. Nanocomposites preparation	21
7. Melt-spinning process	23
8. Nanocomposites characterization	26
8.1 Electrical conductivity measurements	26
8.2 Melt flow index characterization	27

8.3 Heating tests by Joule Effect	28
8.4 Morphological characterization	30
9. Multifilaments characterization	32
9.1 Electrical characterization	32
9.2 Mechanical characterization	33
9.3 Joule heating tests for multifilaments	34
IV. Results and Discussion	35
10. Characterization of PBT/CNTs nanocomposites	35
10.1 Study of the electrical percolation threshold	35
10.2 Heating evaluation	36
10.3 Melt flow index	37
10.4 Macrodispersion	38
11. Influence of graphite addition	40
11.1 Electrical conductivity	40
11.2 Macrodispersion	41
12. Multifilaments characterization	43
12.1 Electrical conductivity	43
12.2 Mechanical characterization	46
12.3 Heating evaluation	47
V. Conclusions	48
13. Proposal for future work	49
IV. Bibliography	50
V. Appendix	57
1. Materials technical datasheet	57
1.1 PBT DuPont™ Crastin® FGS600F40 NC010	57
1.2 NANOCYL® NC7000™ MWCNTs technical datasheet	63

1.3 Graphite GraphTHERM® 23/99.9 technical datasheet	64
1.4 CI 1036 Highly Conductive Silver Ink technical datasheet	65
2. Characterization data	67
2.1 Melt flow index data	67
2.2 Mechanical tests data	68
2.3 Electrical characterization data	72
2.4 Heating tests data	81

List of Figures

Figure 1 – Typical values of electrical conductivity of commonly known materials. Taken from [20].	7
Figure 2 – Schematic representation of carbon allotropes: Graphite, graphene, and carbon nanotube. Taken from [21].	7
Figure 3 – Theoretical behavior of the electrical resistivity with increasing filler concentration. Taken from [25].	8
Figure 4 – a) Thermal conductivity and b) electrical conductivity comparisons between binary and ternary composites. Taken from [3].	10
Figure 5 – Schematic representation of CNTs dispersion mechanisms: a) rupture; b) erosion. Taken from [37].	13
Figure 6 – Schematic representation of a melt-spinning line. Polymer is represented in yellow (reproduced from [42]).	14
Figure 7 – Chemical structure of PBT. Taken from [52].	17
Figure 8 – Simple structural representation of carbon nanotubes. Rolling one or several (a) sheets of graphene forms (b) SWCNTs, (c) DWCNTs and (d) MWCNTs. Adapted from [61].	18
Figure 9 - Schematic illustration of graphite structure. Taken from [63].	19
Figure 10 – Corotating twin-screw extruder by Rondol Technology Ltd, 21 mm.	21
Figure 11 – Schematic representation of the melt-spinning extruder.	24
Figure 12 - Samples used for the electrical characterization.	26
Figure 13 – Setup used for the thermal characterization tests of the nanocomposites.	28
Figure 14 – Representative images of the setup used for the heating measurements.	29
Figure 15 – Example of cross-section image of PBT/2%CNTs/5%G.	30
Figure 16 - Color gradient applied to the sample. Every red dot is an agglomerate.	31
Figure 17 – Setup used for the electrical characterization of the multifilaments.	32
Figure 18 - Representative image of the measurement of the longitudinal cross-section geometry of the multifilaments.	33
Figure 19 – Setup used for the thermal characterization of the multifilaments: a) acrylic part and b) final setup.	34
Figure 20 – Electrical conductivity as a function of MWCNTs concentration.	35

Figure 21 – Temperature variation over time during the Joule heating tests for the PBT/3%CNTs.	36
Figure 22 – Comparison between melt flow rate values of the neat polymer and the nanocomposite.	37
Figure 23 – Images obtained with OM of the PBT/3% nanocomposite (magnification 20x). ...	38
Figure 24 – Number of agglomerates (per mm ²) as a function of the area of agglomerates of the PBT/3%CNTs nanocomposite.	39
Figure 25 – Electrical conductivity as a function of graphite concentration (purple line represents the ternary nanocomposites with 1 processing; blue line represents the hybrid nanocomposites with 2 processing steps).	40
Figure 26 – Representative images obtain by OM of the ternary nanocomposites (magnification 20x): a) PBT/2%CNTs/1%G; b) PBT/2%CNTs/5%G.	41
Figure 27 – Number of agglomerates (per mm ²) as a function of the agglomerate areas of the analyzed hybrid nanocomposites.	42
Figure 28 – Electrical conductivity of each multifilament fiber produced.	43
Figure 29 – Elongation at break and tenacity results for the fibers produced under each set of conditions.	46
Figure 30 – Temperature variation over time during the Joule heating tests for the multifilaments.	47

List of Tables

Table 1 - Summary of the articles analyzed for the electrical conductivity in nanocomposites,	10
Table 2 – Properties values comparison between SWCNTs and MWCNTs. Adapted from [61].	18
Table 3 – Properties of PBT Crastin® FGS600F40 NC010, obtained from the technical datasheet.	20
Table 4 – Properties of Nanocyl® NC7000™ MWCNTs and graphite GraphTHERM® 23/99.9 based on the technical datasheets.	20
Table 5 – Operating limits of the extruder.	21
Table 6 – Processing conditions of the nanocomposites.	22
Table 7 – Designation and information about the nanocomposites produced in all steps of this work.	23
Table 8 – Temperature profile of the melt-spinning process.	25
Table 9 – Test conditions.	28
Table 10 – Maximum temperature and time taken to reach the target temperature in each test.	36
Table 11 – Process conditions of the multifilaments.	45

Acronyms

AV - Average

CB - Carbon Black

CCVD - Catalytic Chemical Vapor Deposition

CNTs - Carbon Nanotubes

CPC - Conductive Polymer Composites

CV - Coefficient of Variation

DDR - Draw-down Ratio

DWCNTs - Double-walled Carbon Nanotubes

EG - Expanded Graphite

EMI - Electromagnetic Interference

GnPs - Graphene Nanoplatelets

HDPE - High Density Polyethylene

ICP - Intrinsic Conductive Polymer

LDPE - Low Density Polyethylene

MB - Masterbatch

MFI - Melt-flow Index

MFR - Melt-flow Rate

MWCNTs - Multi-walled Carbon Nanotubes

OM - Optical Microscopy

OS - Operation Status

PA12 - Polyamide 12

PBT - Poly(butylene terephthalate)

PET - Poly(ethylene terephthalate)

PP - Polypropylene

PTT - Poly(trimethylene terephthalate)

SD - Standard Deviation

T_m - Melting Temperature

wt.% - Weight Percentage

I. Introduction

1. Background

Since the beginning of times, mankind found clever and innovative ways to evolve, and this is consequence of the constant evolution we face every day. From our daily tasks to the most complex and challenging assignments, we constantly seek for perfection. As result, the development of new materials like composites, create new technological and scientific opportunities to upgrade equipment or even to improve parts that can have a better overall performance.

The properties obtained in composite materials are ideal to answer these demands. These materials combine complementary properties of its constituents, which cannot be achieved with the isolated components [1]. Thanks to their light weight, corrosion resistance and easy processability, polymer composites are being used in several applications such as power electronics, electric motors and generators, heat exchangers, automotive, military and so on [1], [2].

Polymeric materials are known to have excellent mechanical properties despite being electrically insulating. Therefore, it is necessary to combine them with a conductive filler in order to obtain a conductive polymer composite. Carbon nanoparticles such as carbon nanotubes (CNTs), graphene, graphite, and carbon black (CB) have shown a positive impact in the electrical properties of polymeric composites [3].

These highly conductive fillers can not only turn an insulating polymer into an electrically conductive composite, but also give them the ability to transfer heat, by the Joule heating effect. The passage of electrical current through a conductive nanocomposite can also produce heat adding new functionalities and enabling new areas of application such as sports, healthcare, transportation, and automobiles [4].

However, the dispersion of nanoparticles is the biggest issue involving the performance of the composites. There is a wide variety of articles covering this topic because both electrical and thermal conductivity are significantly affected by the degree of dispersion of the conductive fillers in the matrix [2]. Dispersion is also critical when producing polymeric fibers using the melt-

spinning technique since the spinneret is composed of several holes in the micrometer range and the appearance of agglomerates will cause the fibers to break and will also affect the stretching given by the take-up rolls [5].

Although there has been a considerable number of studies on thermally conductive composites, this research does not extend to conductive melt-spun fibers, which motivated the development of this work.

2. Objectives and Work Planning

The main objective of this work is the development and further characterization of polymer/nanoparticle composites with electrical conductivity using melt extrusion, and to produce multifilament fibers with this composite by multifilament extrusion using the melt-spinning technique and characterization of the Joule heating effect for heated car seats. The work was divided into the following steps:

- 1.** Literature review of the most promising applications for the use of these thermally conductive fibers. Material selection, process parameters (melt compounding and melt-spinning) and characterization methods;
- 2.** Planning definition of the work in progress, in order to define the necessary steps for the fulfillment of the established objectives;
- 3.** Development of the electrically conductive nanocomposites by melt compounding:
 - 3.1** Determination of the electrical percolation threshold of PBT/MWCNTs nanocomposites (production of nanocomposites with 1 wt.% to 5 wt.%);
 - 3.2** Production of hybrid nanocomposites PBT/MWCNTs/Graphite to study possible synergy between both fillers;
- 4.** Thermal and rheological characterization of the nanocomposites in order to evaluate if they meet the requirements for the melt-spinning process;
- 5.** Production of thermally conductive multifilament fibers by melt-spinning;
- 6.** Characterization and validation of the electrical, thermal, and mechanical properties of the fibers.

3. Dissertation Structure

This work is composed of five chapters.

The first chapter covers a brief introduction to the work, consisting of the background, the objectives and organization of this dissertation.

The second chapter describes the characteristics and main properties of PBT, carbon nanotubes, and graphite, as well as a literature review of the theoretical principles of production and characterization of polymeric nanocomposites. A compilation of studies on the production of nanocomposites filled with conductive nanoparticles is also described in this chapter.

The third chapter lists the materials and equipment's used in the production of these nanocomposites, as well as a description of the experimental characterization techniques used.

The fourth chapter presents and analyzes the experimental results obtained.

Lastly, the fifth chapter presents the main conclusions from the work done, as well as proposals for future work.

II. Literature Review

4. State of art

Composite materials combine the properties of its constituents, producing a new material and allowing it to have strengths from both of them while often overcoming their weaknesses. Composites are commonly identified by the type of matrix that holds the filler together. These composites can have a metallic, ceramic, or polymeric matrix [6].

Since polymers have excellent mechanical properties, good processability and elevated corrosion resistance they are seen as a good option to replace metals and other materials in very distinct applications such as construction, military, automotive, aerospace and so on [1].

Generally, polymeric materials are known to be thermal and electrically insulating ($<0,5$ W/mK, $\approx 10^{15}$ Ω .cm, respectively). However, thermal conductivity is one of the most important properties in many applications and it is getting considerable attention. Despite existing many strategies to enhance the thermal conductivity of polymers, the most efficient way is to combine conductive fillers within the polymer matrix [3]. The incorporation of these fillers in insulating matrixes can reduce their volume resistivity as well as increase thermal conductivity while improving mechanical, chemical, and thermal properties. Therefore, materials like polypropylene (PP), low-density polyethylene (LDPE), high-density polyethylene (HDPE), polyethylene terephthalate (PET) among other polymers have been widely used to create thermally conductive composites [7], [8] when combined with conductive fillers, especially carbon-based fillers such as graphite, graphene, carbon nanotubes or carbon black [9].

When the filler has at least one dimension below approximately 100 nm, it can be classified as a nanocomposite [10]. To ensure a reliable performance of the nanocomposites it is essential to establish a strong interfacial adhesion and a proper dispersion between matrix and filler [11].

Melt spun multifilament fibers are known to have a wide variety of properties that can be used in different industries like textile (underwear, sportswear, and fabrics), automotive (seat belts), sports equipment (climbing ropes and racquet strings) and fishing lines. Among the benefits of these fibers, the mechanical and electrical properties are the most important ones. There are several procedures to create electrically conductive fibers, for example using an intrinsic conductive polymer (ICP), melt mixing an insulating polymer with conductive fillers

(carbon black, graphite, carbon nanotubes, etc.) or even coating a fiber with conductive materials. However, the incorporation of conductive nanofillers has gained a lot of interest due to the quickness and ease of the process [12], [13].

4.1. Nanocomposites

Currently, emerging industries are looking for new thermally conductive materials to replace, for example, metals in parts that require heat dissipation. Since polymer composites are somewhat easy to process and can be integrated in parts with complex geometry, are lightweight, and have a good corrosion resistance they are suitable for areas like LED devices, electronic assembly and packaging, battery, and solar applications [14].

Polymer nanocomposites can be produced using three distinct methods: melt compounding, *in situ* polymerization or solution mixing [15]. Solution mixing is a process where the nanoparticles are dispersed into polymer solutions through ultrasonication and shearing depending on the solubility of the respective particles in the solvents [16]. On *in situ* polymerization the nanoparticles are previously dispersed in a monomer solution and then the nanocomposite material is formed via standard polymerization procedures [17]. Lastly, the melt compounding process is the most popular method to produce nanocomposites by virtue of being environmentally friendly (does not require organic solvents) and its compatibility to a large-scale production. This technique consists in combining the melted polymer with the desired nanoparticle by means of an extruder [18]. Despite of all the advantages of the melt compounding process, the main disadvantage is the limitations to the dispersion of the filler in the polymer melt, with higher viscosity compared to solution methods [19].

4.2. Conductive fillers

Metals (or conductive materials) are known to have high electrical conductivity making them extremely important in electronic areas. Semiconductor materials include the nanocomposites since they are highly dependent of the type of filler and its concentration on the matrix. These materials represent an intermediate state between conductors and insulators. Finally, insulators (e.g. polymers) are materials that block the passage of electrical current because of their high resistivity. The typical electrical conductivity values (in S/m) of each class of materials can be seen in Figure 1.

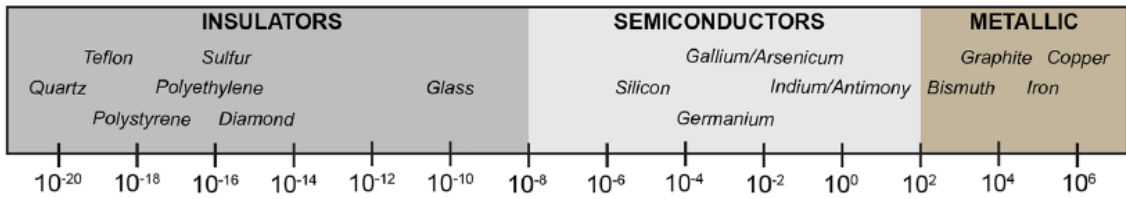


Figure 1 – Typical values of electrical conductivity of commonly known materials. Taken from [20].

Electrical conductivity is one of the most important properties when producing nanocomposites with heat conduction. Therefore, to create conductive polymer composites it is necessary to introduce highly conductive fillers into their matrix [14]. These fillers can be classified into three distinct categories depending on their constituent material: carbon-based, metallic, and ceramic. Carbon-based fillers include carbon nanotubes, graphite, graphene, and carbon black (Figure 2) [15]. Carbon nanoparticles have shown a positive impact in physical and chemical properties, emphasizing the improvement in mechanical, thermal, and electrical properties [3], [22]-[23].

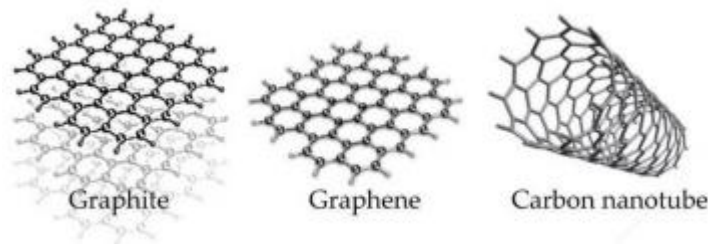


Figure 2 – Schematic representation of carbon allotropes: Graphite, graphene, and carbon nanotube. Taken from [21].

4.3. Electrical conductivity in nanocomposites

The percolation threshold (Figure 3) is described by the critical conductive filler content where an insulating material becomes conductive. When this critical filler concentration is achieved, a continuous network is created where the electrical current can pass through [24]. Given the problems of dispersion it is important that the percolation threshold is reached with the lowest possible filler concentration to prevent the appearance of agglomerates [5].

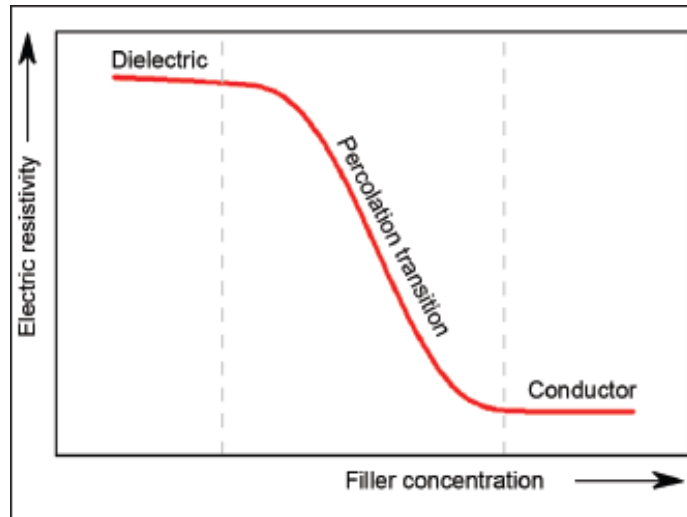


Figure 3 – Theoretical behavior of the electrical resistivity with increasing filler concentration. Taken from [25].

Several studies have been conducted in order to study the electrical percolation threshold of carbon nanoparticles in polymer composites and some will be presented below.

Seo *et al.* [26] produced polypropylene (PP) and MWCNTs nanocomposites and obtained a percolation threshold between 1 and 2 wt.% of MWCNTs and were able to decrease the volume resistivity from approximately 10^7 Ohm.cm to 10^2 Ohm.cm, respectively. Above 2 wt.%, the volume resistivity was maintained even with nanocomposites with 5 wt.% of MWCNTs. Zhang *et al.* [27] prepared composites of HDPE (high density polyethylene) and SWCNTs using spray coating. The electrical conductivity of neat HDPE is 1×10^{-14} S/cm and this value increased drastically by adding a filler content of 4 wt.% of SWCNTs reaching 1×10^{-5} S/cm. Over 6 wt.% of SWCNTs, the electrical conductivity tended to stabilize. Hu *et al.* [28] investigated the percolation threshold of a PET/MWCNTs composites. The electrical conductivity of neat PET is $8,6 \times 10^{-17}$ S/cm and it was possible to achieve 10^{-5} S/cm with just 2 wt.% of MWCNTs. The low percolation threshold of this composite is explained by the high aspect ratio of the MWCNTs and their homogenous dispersion in PET matrix. With a filler content of 1 wt.%, the composite exceeded the antistatic criterion for thin films. Allaoui *et al.* [29] dispersed MWCNTs in an epoxy polymer matrix. The value of percolation threshold of this composite was between 0,5 and 1 wt.% obtaining a value of 1×10^{-3} S/cm with a filler loading of 1 wt.%. Composites with 4 wt.% only improved the conductivity value by an order of magnitude. This high MWCNTs content would negatively affect the mechanical properties of the overall composite achieving a “saturation effect.” Dorigato *et al.* [30] prepared PBT/MWCNTs using the melt compounding process and

were able to decrease the electrical resistivity of neat PBT from 10^{15} to 10^4 Ω .cm with 0,5 wt.% of MWCNTs. For the PBT/3%MWCNTs nanocomposites, the value of resistivity only reduced by two orders of magnitude achieving a percolation threshold below 0,5 wt.%. Dorigato *et al.* [31] conducted a previous study on PBT/MWCNTs and were not able to reach this type of values. This time, only with a filler content of 6 wt.% of MWCNTs it was possible to reach a value of 10^3 Ω .cm. Moreover, regarding the carbon black nanocomposites, it was possible to achieve a value of 10^4 Ω .cm but with a 15 wt.% of CB. These values were not as satisfactory as their previous study probably due to the use of a twin-screw extruder in this more recent work which led to a better filler dispersion within the PBT matrix.

Hybrid nanocomposites are thought to enhance thermal conductivity through the synergistic effect of both fillers. Che *et al.* [3] prepared ternary composites using high density polyethylene (HDPE), expanded graphite (EG) and multi-walled carbon nanotubes. Two different binary composites (HDPE/CNTs and HDPE/EG) were produced to study both electrical and thermal conductivity. It was observed that with a low filler content of CNTs (2,5 wt.%) was possible to reach values of electrical conductivity of approximately 10^1 S/m. On the other hand, to get the same value of electrical conductivity with EG it was needed a much larger filler content (around 25 wt.%). Concerning the thermal conductivity, the opposite effect occurs. HDPE/EG reaches greater values of thermal conductivity ($\approx 2,25$ W/mK with 20 wt.%) when compared with HDPE/CNTs ($\approx 1,0$ W/mK with 20 wt.%). Taking that into consideration, ternary composites were prepared fixing the EG content in 10, 15 and 20 wt.% and adding small concentrations of CNTs to study their electrical and thermal conductivity. In summary, these ternary composites were able to increase both conductivities due to great synergy between both carbon nanoparticles and graphite as shown in Figure 4.

Table 1 summarizes the research done regarding the electrical conductivity in polymer nanocomposites.

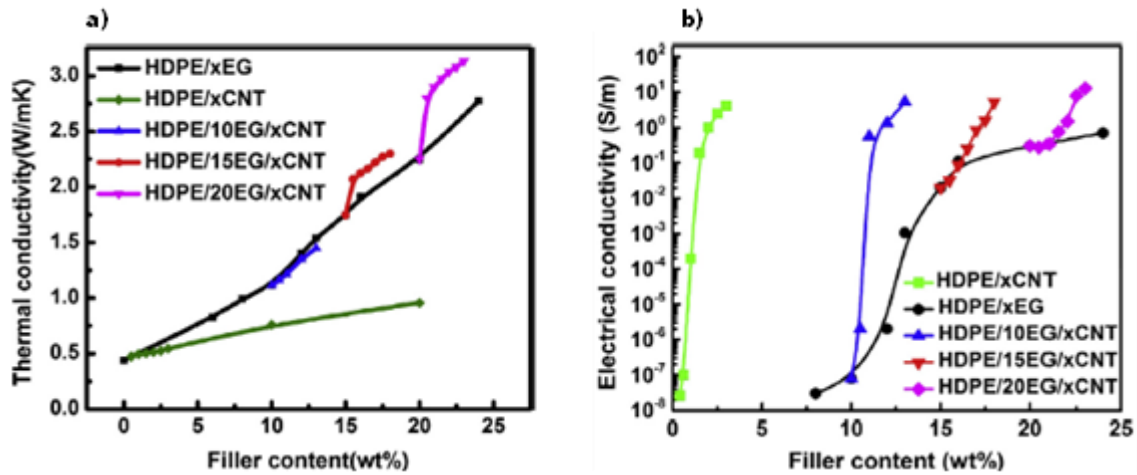


Figure 4 – a) Thermal conductivity and b) electrical conductivity comparisons between binary and ternary composites. Taken from [3].

Table 1 - Summary of the articles analyzed for the electrical conductivity in nanocomposites,

Matrix	Filler	Electrical Percolation Threshold	Electrical Resistivity/Conductivity	Processing Technique	Reference
PP	MWCNTs	1 – 2 wt. %	$10^7 - 10^2 \Omega \cdot \text{cm}$	Melt compounding	[26]
HDPE	SWCNTs	4 wt. %	$1 \times 10^{-5} \text{ S/cm}$	Melt compounding	[27]
PET	MWCNTs	0,5 – 1 wt. %	10^{-9} S/cm	Solution mixing	[28]
Epoxy	MWCNTs	0,5 – 1 wt. %	$1 \times 10^{-3} \text{ S/cm}$	Solution mixing	[29]
PBT	MWCNTs	0,5 wt. %	$10^{15} - 10^4 \Omega \cdot \text{cm}$	Melt compounding	[30]
PBT	MWCNTs and CB	2 – 3 wt. % (MWCNTs) 10 – 13 wt. % (CB)	$10^6 \Omega \cdot \text{cm}$ (MWCNTs) $10^5 \Omega \cdot \text{cm}$ (CB)	Melt compounding	[31]
HDPE	MWCNTs and EG	1,5 wt. % (MWCNTs) 15 wt. % (EG)	10^1 S/m 10^0 S/m	Melt compounding	[3]

4.4. Heat conduction in nanocomposites and multifilaments

Thermal conductivity is a property that is getting greater attention. The heating of a nanocomposite is strongly influenced by the properties of the nanofiller [32]. Thermally conductive nanocomposites can be used in applications where the generation of heat is needed such as for de-icing [33] and self-repairing composites by applying electrical current [34].

The electrical current that crosses an electrically conductive nanocomposite can generate heat by the Joule effect. The Joule heating effect was described by James Joule in 1841 as the generation of heat when an electrical current goes through a conductive material. This happens when electrons collide with the atomic network of conductive materials, transferring kinetic energy in form of dissipated heat. For this phenomenon to occur it is crucial that the material is electrical and thermally conductive [35].

Even though it is not a very in-depth topic, some studies have been conducted about the heat conduction in nanocomposites by the Joule heating effect. Savinada *et al.* [36] produced thin films creating a conductive paste by combining polyurethane-based resins with graphene nanoplatelets (GnPs) and MWCNTs and coated a cotton substrate using screen-printing. The final result was a coated cotton fabric that was able to reach values of electrical conductivity of 1×10^1 S/m with a filler content of 5 wt.% (CNTs + GNPs). Afterwards, the Joule heating effect was tested by applying a voltage of 12V, commonly used in automotive applications, reaching a temperature of 42,7 °C. Equally, Prolongo *et al.* [32] processed composites with an epoxy resin combined with graphene nanoplatelets and CNTs. The epoxy/CNTs composites reached an electrical conductivity value of 0,2 S/m with a filler content of 0,5 wt.% while the epoxy/GnPs composites reached a value of 0,004 S/m with a concentration of 8 wt.%. Regarding the Joule heating tests, both composites were able to reach a temperature close to 75 °C, but with different voltages, 75 V for the composite with 0,25 wt.% CNTs and 200 V for the composite with 8 wt.% GNPs. That said, it is imperative to reach a compromise between electrical and thermal conductivity in order for the Joule effect to work effectively.

According to what was previously stated, the Joule heating effect is applicable to polymer nanocomposites, but it is essential that all the processing conditions are set in order to maximize the properties provided by the nanoparticles.

4.5. Dispersion of carbon nanoparticles

To achieve the maximized properties of nanocomposites it is imperative that the filler is well dispersed in the polymeric matrix. However, this dispersion is challenging to achieve due to the fillers tendency to form agglomerates and their weak interfacial adhesion with the polymer matrix. These agglomerates are typically held by strong Van der Waals interactions and physical entanglements between proximal nanoparticles [38]. In order to deal with this problem, several methods of dispersion and functionalization have been developed such as ultrasonication, calendaring process, ball milling, and physical or chemical functionalization [11]. The use of masterbatches (composites with high filler content) are also an effective way to improve dispersion and homogenization due to the need of reprocessing with neat polymer to obtain the target percentage of nanoparticle in the matrix. The dilution process allows the agglomerates to be submitted to a second shear force which, in several cases, turns out to enhance the dispersion of the nanoparticles [38]. Moreover, twin-screw extruders provide a better dispersion than single-screw extruders [39] as well as the use of some additives that can decrease the interfacial force between polymer and nanoparticle, producing a homogeneous mixture [38]. Thus, optimizing the processing conditions for nanocomposites is critical, since the state of dispersion of the nanoparticles influences their electrical conductivity, especially in concentrations near the electrical percolation threshold [40].

In particular, carbon nanotubes dispersion has been getting considerable attention. In polymer/CNTs nanocomposites, the dispersion of CNTs can be explained by two mechanisms (Figure 5): rupture and erosion [38]. Rupture consists in a fast process where occurs the successive breakage of the agglomerates into smaller ones until each nanotube is individually separated. Erosion involves the detachment of CNTs (or small agglomerates of CNTs) from the surface of larger agglomerate clusters into the polymer melt [37].

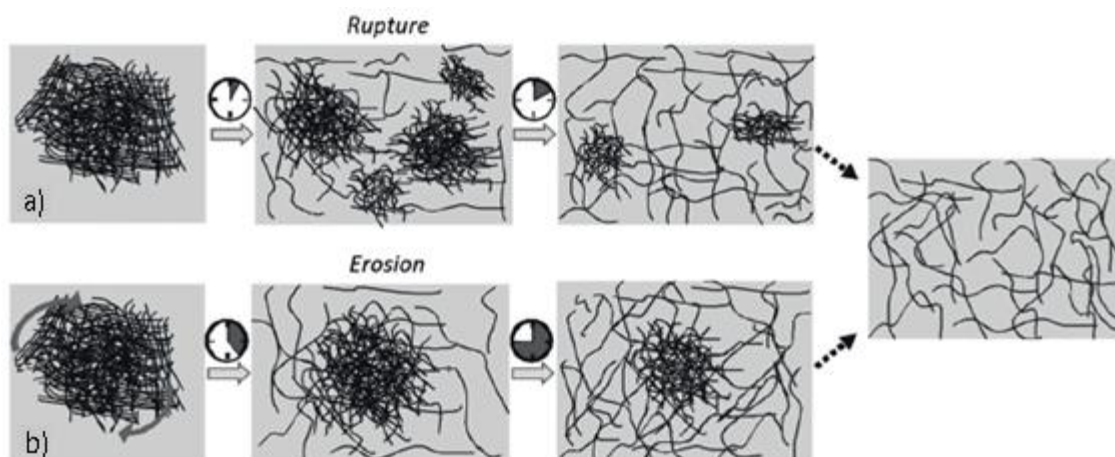


Figure 5 – Schematic representation of CNTs dispersion mechanisms: a) rupture; b) erosion. Taken from [37].

In the melt compounding process, the dispersion of CNTs can be affected by a multitude of parameters, especially the processing conditions and the extruder configuration (single-screw or twin-screw) for example the screw configuration, throughput, temperature profile, and screw rotation speed have a major effect in shear stress generated and, consequently, in the quality of the nanocomposite.

It was determined that higher screw rotation speed resulted in the formation of fewer agglomerates because of the higher shear stress that is applied to the molten material which enables the rupture mechanism. Though, extremely high shear stress will promote nanotubes breakage and consequently decrease their aspect ratio. Alternatively, low shear stress induces the erosion mechanism due to low viscosity of the melt and high residence times [37], [38], [41]. Thus, it is fundamental to optimize the processing conditions of nanocomposites since the dispersion of carbon nanotubes have a significant impact on their electrical and thermal conductivity [2].

4.6. Melt-spinning technique

When processing polymer fibers through melt-spinning, it is important to take into consideration the presence of agglomerates. They are detrimental to the melt spinning process, however they may appear in small numbers and, most importantly, with dimensions lower than the melt-spinning die diameter. This technique can be described as a process where a thermoplastic polymer is heated above its T_m (melting temperature) and extruded by pumping it

through a die formed by a set of holes with diameter in the micrometer range to form molten multifilaments. The polymer (in pellet form) is fed to the extruder from a hopper. The screw extruder has distinct heating zones that sequentially heat the material above its melting point. Then, a polymer melt is fed to the metering pump while maintaining it above T_m . The pump is coupled with a spin pack that is composed of a stack of circular plates and metal filters between them. Each of them has several holes through which the polymer melt flows until reaching the spinneret. After leaving the spinneret, these multifilaments are cooled with a quenching chamber or water bath while being pulled down at a faster speed than the melt flow and the ratio of this speed is called draw-down ratio (DDR) [42], [43]. Lastly, the multifilaments are wound up on a bobbin. A standard melt-spinning line include a screw extruder, a spin pack, and a filament draw-down unit, as illustrated in Figure 6 [42].

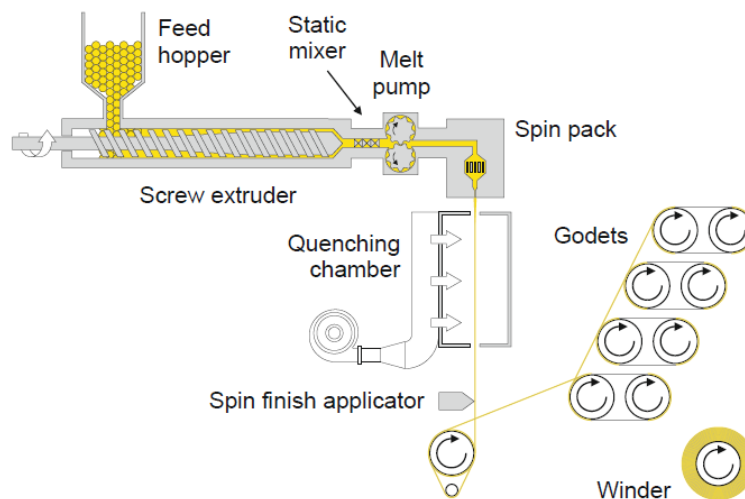


Figure 6 – Schematic representation of a melt-spinning line. Polymer is represented in yellow (reproduced from [42]).

Since the holes of spinning pack are comprised in the micrometer range, it is imperative that the material used is homogeneous, because the occurrence of agglomerates above 5% of the multifilament diameter will cause obstruction of the filters and, subsequently, irregularity of the filaments flow, which can lead to fibers breakage [5], [42].

It is fundamental to understand how the melt-spinning process can affect the electrical properties of the multifilaments. The drawing powered by the feeding and drawing roll induce the molecular orientation of the polymer matrix and the nanoparticles, directly affecting the conductive network and, consequently, the electrical conductivity. Thus, the increase of drawing

speed will enhance the orientation of the MWCNTs along the multifilaments [5]. This increased orientation will drastically improve the final mechanical properties of the multifilament [44]. On the other hand, the increase of the drawing ratio may separate the nanoparticles from each other, eventually decreasing the density of the conductive network and, therefore, the electrical conductivity [45].

Bouchard *et al.* [44] added MWCNTs to a matrix of poly(hydroxy ether) of bisphenol A to evaluate their electrical properties. It was concluded the drawing of the multifilaments have a significant impact on the electrical conductivity. This resulted in a decrease of the electrical conductivity by 10 orders of magnitude ($4,50 \times 10^{-1}$ to $3,55 \times 10^{-11}$ S/m) when comparing the melt compounded composite to the melt-spun multifilaments with the same filler content of 1,5 wt.%. This situation can be solved by reaching a compromise between concentration and dispersion.

Moreover, Marischal *et al.* [45] prepared composites of polyamide 12 (PA12) filled with carbon black to study the influence of the melt-spinning parameters in the electrical conductivity of the multifilaments. It was observed that the electrical conductivity is severely affected by the output of the volumetric pump because it is related to the internal shear stress. The internal shear stress triggers the destruction of the agglomerates and a consequent alignment of the fillers. Nevertheless, value of output of the volumetric pump lower than $50 \text{ cm}^3/\text{min}$ leads to the separation of the fillers and a consequent destruction of the conductive path. On top of that, they concluded that the orientation of the fillers can also change the mechanical properties of the fibers. While in a semi-solid state, the increase of the drawing out roll speed causes a filler orientation which enhances the mechanical properties but, once again, there is a critical drawing out speed of 2 above which the nanoparticles will distance from each other and break the conductive network.

In conclusion, it is essential to reach a compromise between the filler concentration and the dispersion of the nanoparticles to ensure a stable process and guarantee good electrical and mechanical properties of the final multifilaments.

4.7. Materials selection

Since the main goal is to produce multifilaments with heat conduction properties, it is necessary to select the best materials (polymer matrix and conductive filler) for heated car seats.

As stated previously, carbon nanoparticles (CNTs and graphite) are the best conductive filler for electrical and thermal applications in polymer composites because of their excellent properties such as low density, high elastic modulus, a good thermal stability and, most importantly, outstanding thermal and electrical conductivity [11], [46], [47].

Regarding the polymer matrix, polyesters (PET and PBT), polyolefins (PP, LDPE and HDPE), and polyamides (PA 6 and PA 6.6) are the most commonly used polymers for the melt-spinning technique [42], [48], [49]. Polyolefins are mostly used in medical applications for surgical gowns and masks while the polyamides are particularly used for textile applications. Polyesters can be used in a wider variety of applications and have excellent mechanical, thermal, and chemical properties [42].

Since the crystalline structures favor the electrical conductivity [50] and PBT has a faster, easier and better crystallization rate than PET [22], [42], it makes it more interesting for the electrically conductive nanocomposites.

4.7.1. Poly(butylene terephthalate)

Nowadays, polyesters are among the most economically important classes of polymers. Polyesters can be classified into two types: (i) thermoplastic polyesters and (ii) unsaturated polyesters. The most widely known are the thermoplastic which includes polyethylene terephthalate (PET), poly(trimethylene terephthalate) (PTT) and poly(butylene terephthalate) (PBT) [51].

As previously stated, PBT (Figure 7) is a semicrystalline thermoplastic polyester that appeared in the late 1960s and became a commonly used material because of its easy processability and fast crystallization which makes it suitable for very structural applications like automotive, electrical, and electronic industries. PBT is prepared by polycondensation of 1,4-butanediol with terephthalic acid or dimethyl terephthalate [30], [52], [53].

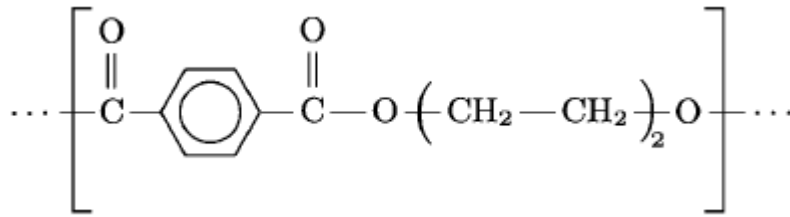


Figure 7 – Chemical structure of PBT. Taken from [52].

PBT-based composites are described by high stiffness and strength, excellent electrical properties, chemical resistance, and low moisture absorption [30]. Additionally, PBT has good electrical and dielectric properties demonstrating particularly good creep current resistance and does not initiate any electrolytic corrosion [52].

This polymer can be blended, mainly, with carbon nanoparticles such as carbon nanotubes, carbon black, graphite, and graphene, forming nanocomposites that can be used in electrically conductive applications [3], [31], [54], [55]. PBT composites can be applied in electronic applications such as EMI shielding [56], in packaging films or sensitive electronic parts [30], but also in the automotive and medical industries [22].

4.7.2. Carbon nanotubes

In 1991, Sumio Iijima was one of the pioneers of the modern technology for the production of carbon nanotubes [57]. Since its discovery, CNTs have been studied and further developed [58] becoming particularly useful in a wide range of applications including reinforcing fibers, electromagnetic shields, smart clothing [12], sensors, electronics on flexible substrates, etc. [59]. The excellent properties of carbon nanotubes (Table 2) make them an extremely versatile filler due to low density (0,8 - 1,8 g/cm³), high electrical and thermal conductivity (10²- 10⁶ S/cm and 2000 - 6000 W/mK, respectively), excellent thermal stability (up to 2800 °C), and extraordinary Young's modulus (1-2 TPa) [11], [60].

Table 2 – Properties values comparison between SWCNTs and MWCNTs. Adapted from [61].

Properties	SWCNTs	MWCNTs
Relative density (g/cm ³)	0,8 – 1,3	1,8 – 2,6
Specific area (m ² /g)	400 – 900	200 – 400
Young's modulus (Pa)	≈ 1000	≈ 1000
Tensile strength (Pa)	(3 – 50) x 10 ¹⁰	(1 – 15) x 10 ¹⁰
Thermal conductivity (W/mK)	3000 – 6000	2000 – 3000
Electrical conductivity (S/cm)	10 ² – 10 ⁶	10 ³ – 10 ⁵
Thermal stability temperature in air (°C)	550 – 650	550 – 650

CNTs can be structurally classified in three distinct types (Figure 8): single-walled carbon nanotubes (SWCNTs), double-walled carbon nanotubes (DWCNTs) and multi-walled carbon nanotubes (MWCNTs). As the name suggests, SWCNTs are composed of single layer of graphene sheet rolled up around itself while DWCNTs are made of two layers of graphene and MWCNTs consist in three or more layers rolled up concentrically [59].

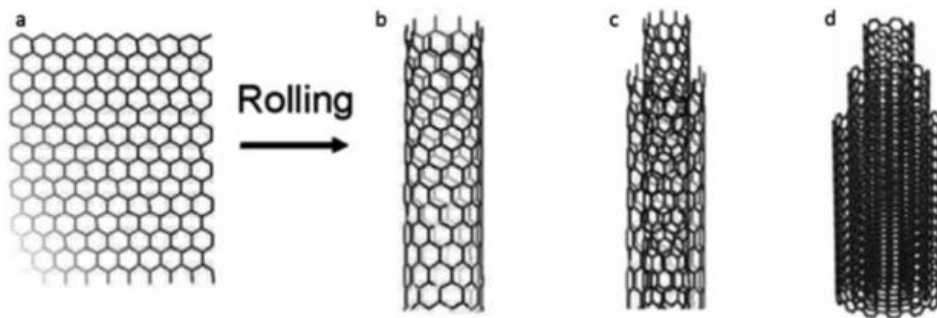


Figure 8 – Simple structural representation of carbon nanotubes. Rolling one or several (a) sheets of graphene forms (b) SWCNTs, (c) DWCNTs and (d) MWCNTs. Adapted from [61].

4.7.3. Graphite

Graphite (Figure 9) is a carbon filler that exists naturally but can equally be synthetically produced. Structurally, it consists of thousands of parallel layers of graphene sheets with sp^2 -hybridized carbon bonded hexagonally which are held together through Van der Waals forces. Therefore, graphite has excellent properties including its elastic modulus (1TPa), low electrical resistivity ($\approx 50 \mu\Omega\text{cm}$ at room temperature) [46], high thermal and electrical conductivity (5300 W/mK and 10^4 S/cm) [47], and excellent thermal stability under inert atmosphere and in the vacuum.

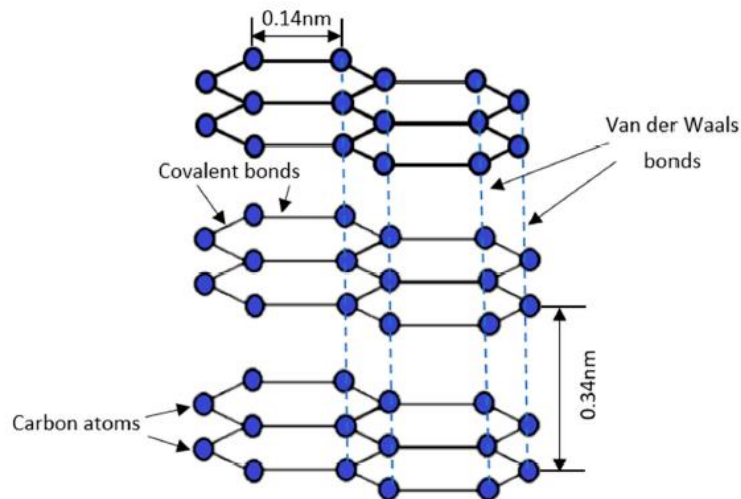


Figure 9 - Schematic illustration of graphite structure. Taken from [63].

III. Materials and Methods

5. Materials

The polymer matrix used was a low viscosity poly(butylene terephthalate) (PBT), grade Crastin® FGS600F40 NC010, provided by Dupont. The relevant properties of the material are shown in Table 3.

Table 3 – Properties of PBT Crastin® FGS600F40 NC010, obtained from the technical datasheet.

PBT	
Melt flow rate (g/ 10 min)	33
Tensile Modulus (MPa)	2400
Melting temperature (°C)	223
Glass transition temperature (°C)	55
Density (g/cm³)	1,29
Volume resistivity (Ω.cm)	1 x 10 ¹⁶
Water absorption (%)	0,4

The nanofillers used, both in powder form, were NANOCYL® NC7000™ MWCNTs (multi-wall carbon nanotubes) produced by catalytic chemical vapor deposition (CCVD), supplied by Nanocyl S.A, and graphite, grade GraphTHERM® 23/99.9 supplied by LUH. Their relevant properties are represented in Table 4:

Table 4 – Properties of Nanocyl® NC7000™ MWCNTs and graphite GraphTHERM® 23/99.9 based on the technical datasheets.

MWCNTs		Graphite	
Average diameter (nm)	9,5	Carbon content (%)	99,9
Average length (µm)	1,5	Ash (%)	0,1
Carbon purity (%)	90	Moisture (%)	0,5
Surface area (m²/g)	250 – 300	Surface area (m²/g)	5 – 6,5
Volume resistivity (Ω.cm)	10 ⁻⁴	Tamped density (g/cm³)	0,95 – 1,05
Thermal conductivity (W/mK)	3000	Size (µm)	10 – 50

6. Nanocomposites preparation

The nanocomposites were prepared by melt compounding using a corotating twin-screw extruder (Figure 10) with a screw diameter of 21 mm and a length to diameter ratio (L/D) of 25 from Rondol Technology Ltd. This screw configuration used two chaotic mixture screws. The extruder is made up of four heating zones along the length of the cylinder, excluding the spinneret, and peripheral feeders. The extruded filament was then cooled in a water bath and collected for further characterization. The operating limits of the extruder used are presented in Table 5.



Figure 10 – Corotating twin-screw extruder by Rondol Technology Ltd, 21 mm.

Table 5 – Operating limits of the extruder.

Condition	Maximum
Temperature (°C)	450
Screw rotation speed (rpm)	300
Torque (%)	100
Pressure (bar)	90

Prior to processing, the PBT pellets were dried in a dehumidifier Piovan DPC30 at 120 °C for 4h. After the drying process, the humidity of the pellets was measured to ensure the absence of water in the nanocomposite preparation. To ensure a controlled feed rate, two feeders were used – a gravimetric for the MWCNTs powder and a volumetric for the PBT pellets. Since the density of the materials varies depending on the type and percentage of fillers incorporated, the feeders had to be calibrated beforehand to ensure the desired flow rate. The processing conditions (Table 6) were set based on the melting temperature of the PBT (specified in datasheet) and supported with the analysis of previous works that cover identical topics. The screw rotation speed was set to 140 RPM in order prevent backflow of material.

Table 6 – Processing conditions of the nanocomposites.

Condition	Value
Temperature profile (°C)	210, 215, 220, 225, 230
Screw rotation speed (RPM)	140
Feed rate (kg/h)	3
Cooling bath (°C)	50

Firstly, as stated in [38], to help the MWCNTs dispersion, a nanocomposite with a high filler content of 6 wt.% of MWCNTs was produced as a masterbatch to form the nanocomposites with the designated concentrations. The extruded material was cooled in a water bath at 50 °C and pelletized. Then, the PBT/6%CNTs was diluted with neat PBT to produce nanocomposites with lower filler concentration (5; 4; 3,5; 3; 2 and 1 wt.%).

After evaluating the electrical percolation threshold of the PBT/MWCNTs nanocomposites, hybrid nanocomposites were produced by adding three different graphite concentrations. The processing conditions were the same as the binary composites. A high concentration nanocomposite was produced with 5 wt.% of graphite. This composite was cooled in a water bath at 50 °C and then pelletized. Later, the dilution process was performed with neat PBT to create lower filler contents of 1 and 2 wt.% of graphite. From this first processing, a sample of each hybrid nanocomposites (with 1; 2 and 5 wt.% of graphite) were collected to perform the electrical characterization. This filler contents of graphite were selected based on the melt-spinning extruder requirements, since it is not recommended to used nanocomposites with a total filler

content above 7 wt.%. However, to study the effect of a second processing in the electrical conductivity, the ternary nanocomposites were reprocessed because a second shear force could help improve the dispersion. All the nanocomposites produced in this step of the work are presented in Table 7.

Table 7 – Designation and information about the nanocomposites produced in all steps of this work.

	MWCNT content (wt.%)	Graphite content (wt.%)	Nanocomposite name
Step 1 (Masterbatch 6%) 2 processing's	5	-	PBT/5%CNTs
	4	-	PBT/4%CNTs
	3,5	-	PBT/3,5%CNTs
	3	-	PBT/3%CNTs
	2	-	PBT/2%CNTs
	1	-	PBT/1%CNTs
Step 2 (Hybrid nanocomposites) 2 processing's	2	1	PBT/2%CNTs/1%G
	2	2	PBT/2%CNTs/2%G
	2	5	PBT/2%CNTs/5%G
Step 3 (Reprocessed hybrid composites) 3 processing's	2	1	PBT/2%CNTs/1%G (R)
	2	2	PBT/2%CNTs/2%G (R)
	2	5	PBT/2%CNTs/5%G (R)

7. Melt-spinning process

The polymer multifilaments were processed using a single screw multi-component fiber extruder model TRC with a length to diameter ratio (L/D) 30:1 and a pump capacity of 2,9 cm³/rot, from Hills Inc, Co. As Figure 11 suggests, the draw-down ratio DDR is the ratio between the speed of the roll 1 (feeding roll) and the extrusion speed – induces hot stretching. The cold-draw ratio (CDR) is the ratio between the velocity of the stretching roll (roll 2) and the feeding roll. This ratio of speeds causes a cold stretching on the multifilaments. Lastly, between roll 3 (relaxation roll) and roll 2 is where the relaxation of the fiber is applied.

Prior to fiber processing, the PBT with 3 wt.% CNTs and neat PBT were dried in a dehumidifier Piovan DPC30 at 120° C for 4h. Then, the humidity was measured using a Radwag MA 50/1.X2.A.WH moisture analyzer to ensure the effectiveness of the drying process. The melt-spinning equipment is composed by seven heating zones in total: four heating zones along the length of the cylinder plus the pump, transfer line and spinning pack. The temperature profile was set based on the melting temperature of the PBT (specified in datasheet) and in order to ensure a controlled pump pressure (Table 8). The spinning pack used has a mono-component multifilament spinneret with 36 holes with 0,6 mm of diameter each. The process began when the all the parameters were set and the multifilaments started to exit the spinneret. Afterwards, they were cooled by an air quenching chamber and collected by a take-up roll. After, the multifilaments are drawn in two different zones (DDR and CDR) with different temperatures and speeds. Finally, the multifilament was wound in a bobbin (Figure 11).

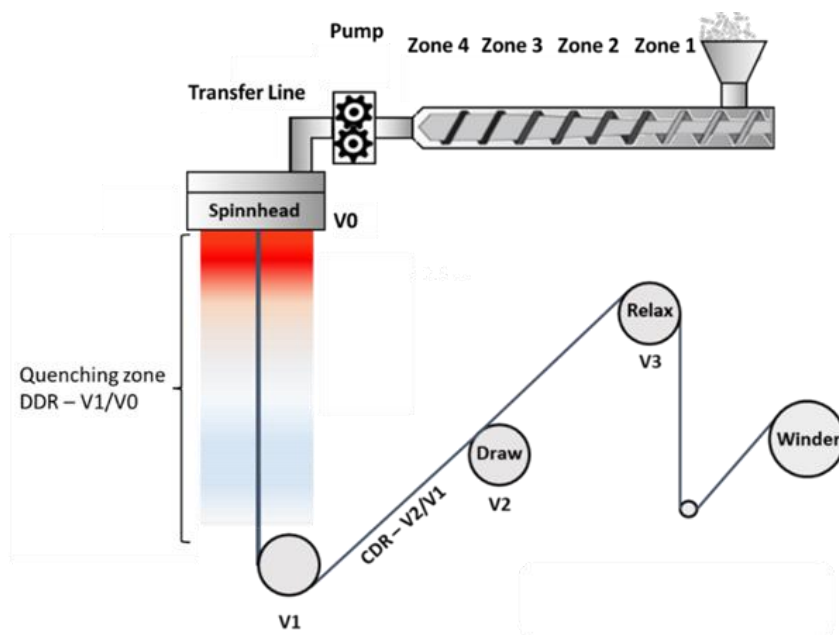


Figure 11 – Schematic representation of the melt-spinning extruder.

Table 8 – Temperature profile of the melt-spinning process.

Zones	Temperature (°C)
Zone 1	215
Zone 2	220
Zone 3	225
Zone 4	235
Pump	240
Transfer Line	215
Spinneret	220

By varying the pump speed, the extrusion speed also changes inducing different DDR and this was done in order to evaluate how the different stretching conditions affect the mechanical properties. The increase of temperature of roll 2 was performed in order to provide mobility for the conductive particles. The other parameters were fixed. The spun fibers were processed with variable pump speeds (10, 14 and 18 rpm), that consequently affected the feed rate. Also, a smaller change in the temperature of the second roll was employed (V2) (40 to 55 °C) while the temperature of the first roll (V1) was set at 60 °C and the third roll (V3) was kept at room temperature.

8. Nanocomposites characterization

8.1 Electrical conductivity measurements

The electrical conductivity of the nanocomposites was measured using the two-probe resistance measurement technique, following the ISO 3915-1981 standard. In this method, a direct current of magnitude (I) is passed between electrodes at the two ends of a strip of the material under test. The voltage drop (ΔU) between two potential electrodes is measured with an electrometer, allowing the measurement of resistance through Equation 1. In this case the resistance was measured by cutting a fixed length of filament and applying a highly conductive silver ink to the cut ends (cross-section) of each sample. The cross-section area was calculated using a caliper to measure the diameter of each sample.

The sample preparation (Figure 12) consists in the cutting of, at least, ten specimens of each nanocomposite with 15 mm of length (d , in Equation 2). Subsequently, silver ink was applied to the ends of each specimen to decrease the contact resistance between the samples and the measurement equipment. The silver ink used was CI 1036 Highly Conductive Silver Ink, needs a thermal cure process in an oven at 120 °C for 20 minutes. Afterwards, the electrical characterization tests were carried out using a sample holder for electrical measurements (Figure 12).



Figure 12 - Samples used for the electrical characterization.

The multimeter used to perform the “two-probe” measurements was a picoamperimeter Keithley 6487. For each measurement, the equipment provides the **volume resistance** (R) based in Ohm’s Law (Equation 1):

$$R = \frac{\Delta U}{I} \quad (1)$$

Since the cross-section area of each sample was known, the **volume resistivity** (ρ) was obtained by means of Equation 2:

$$\rho = \frac{R \cdot A}{d} \quad (2)$$

Lastly, the **electrical conductivity** (σ) was attained by the inverse of resistivity (Equation 3):

$$\sigma = \frac{1}{\rho} \quad (3)$$

8.2 Melt flow index characterization

The MFI characterization was performed using a modular melt flow 7026.000 S/N, CEAST with automatic cut. The melt flow rate is a measure of the ease of flow of melted plastic. The standard designation is Melt Mass-Flow Rate (MFR) expressed in g/10min, following the international standard ASTM D1238. This characterization was performed in order to determine the temperature profile and to evaluate the spinnability of the nanocomposites since previous studies using the same melt-spinning extruder demonstrated that the ideal values of MFI are comprised between 10 and 40 g/min. The tests were conducted under the conditions presented in Table 9.

Table 9 – Test conditions.

Parameters	Conditions
Temperature (°C)	265
Load (kg)	2,16
Pre-heating (s)	60
Initial Weight (g)	8

8.3 Heating tests by Joule Effect

The Joule heating test was carried out by submitting the nanocomposites to an electrical current. To perform these tests, three similar setups (Figure 13) with ten specimens each were assembled, each one with a different nanocomposite. These setups consist of ten filament parts with 2 cm length, placed in parallel with 1,5 cm of distance between each other in order to decrease the resistivity. The filament parts were positioned with both ends on top of a copper tape and then covered with the same highly conductive silver ink used in the electrical conductivity characterization, in order to reduce the overall contact resistance of the setup. After that, the setups were placed in an oven at 120 °C for 20 minutes in order to cure the silver ink.

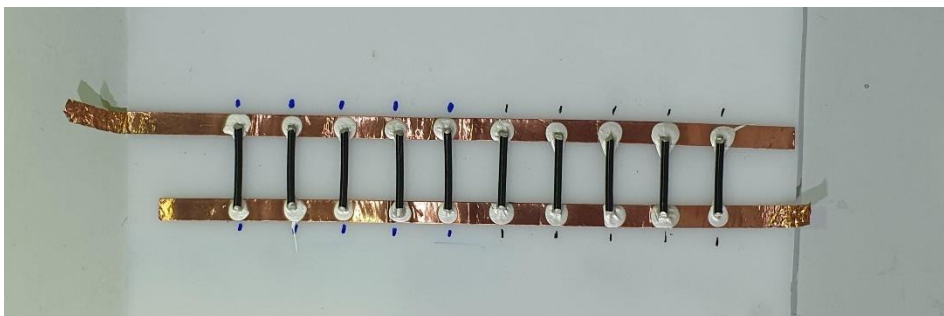


Figure 13 – Setup used for the thermal characterization tests of the nanocomposites.

Prior to the heating tests, the electrical resistivity of each setup was measured with a picoamperimeter Keithley 6487. Afterwards, the heating tests (Figure 14) were performed by connecting a power supply to the two ends of the copper tape and applying three different voltages (12V, 24V and 48V). These voltages were chosen based on the voltage applied by a car battery (12 V) [64], since the main application of the multifilaments is for heated car seats. Also, a target temperature was set between 35 and 40 °C. Each test lasted 5 minutes and the temperature variation was recorded using a FLIR A700 thermal camera. Lastly, the results were analyzed using the FLIR Tools software.

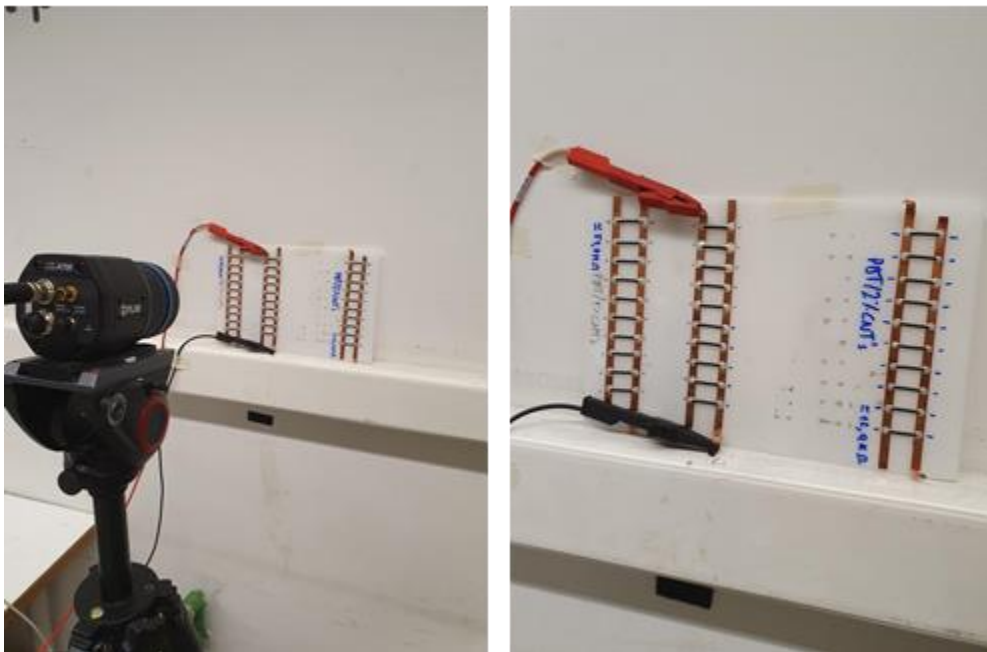


Figure 14 – Representative images of the setup used for the heating measurements.

8.4 Morphological characterization

To study the number and size of the carbon agglomerates in the PBT matrix, the bright-field optical microscopy (OM) was used. This characterization was adapted from the ISO 18553:2002(E).

The samples were prepared by cutting each composite sample on a Leica EM UC6 ultramicrotome. The cross-section of the nanocomposites was cut with approximately 4 μm of thickness. In order to obtain more extensive and precise results, different sections of the nanocomposites were collected and an area of, at least 4 mm^2 , was observed. Afterwards, the samples were immersed in Canada balm, set between a glass slide and a coverslip, and submitted to compression for 24h.

The cross-section images (Figure 15) were captured using a Leica DM2500 M microscope with an ocular of 10x and two objectives of 5x and 10x, using a digital camera Leica K3 C. The images were analyzed with the help of Leica LAS X software.

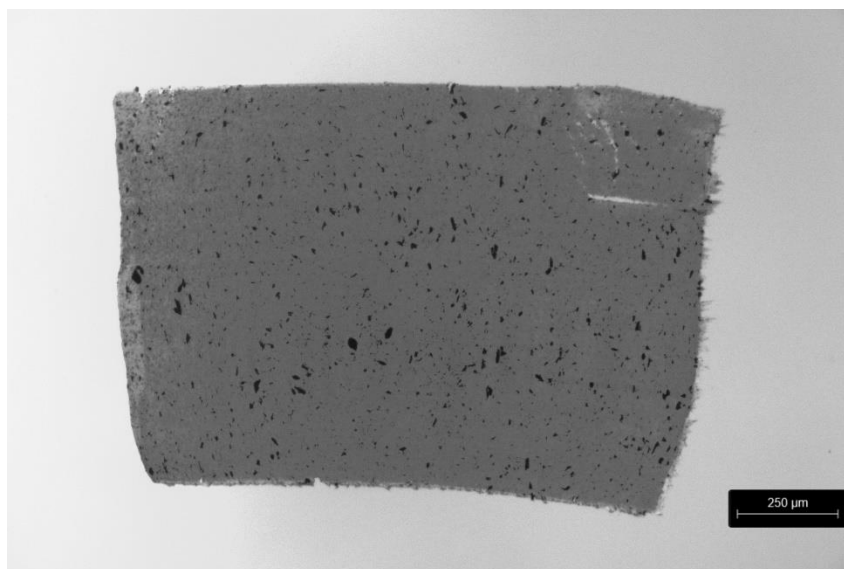


Figure 15 – Example of cross-section image of PBT/2%CNTs/5%G.

Finally, the images were analyzed with the ImageJ software. Firstly, the total area of the sample (in μm^2) was obtained by outlining the edge of the sample. Then, the background of the image was removed and painted in white because the software calculates the area of the agglomerates by using a gradient of colors and every dark zone of the image can be assumed as an agglomerate. Afterwards, the color gradient is applied to the image and adjusted in order to

consider the agglomerates for the calculation (Figure 16). This tool turns every agglomerate into red dots and calculates the area of each one automatically.

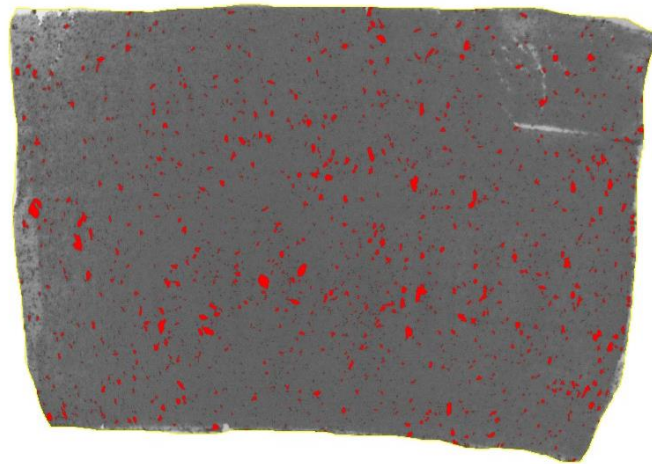


Figure 16 - Color gradient applied to the sample. Every red dot is an agglomerate.

Agglomerates with an area below $5 \mu\text{m}^2$ were disregarded from this analysis [65]. Although the thickness of the observed samples was kept constant, small changes may occur, which are a source of error since the number of agglomerates will vary with the sample volume analyzed.

9. Multifilaments characterization

9.1 Electrical characterization

The electrical characterization of the multifilaments was performed based on the ISO 3915-1981 standard, used for the electrical measurements of the nanocomposites.

In this characterization, five samples of each fiber type were cut with 3 cm length each and placed on a glass slide (Figure 17). Then, twisting was applied to ensure the contact between the multifilaments. Then, the silver ink was applied to both ends (CI 1036 Highly Conductive Silver Ink) to facilitate the contact between the multifilament and the measuring system, before going through a thermal curing process at 120 °C for 20 minutes.

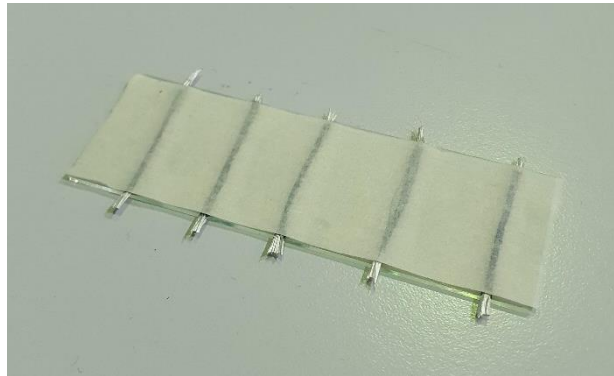


Figure 17 – Setup used for the electrical characterization of the multifilaments.

After carrying out the electrical measurements, to assess fibers longitudinal cross-section geometry (Figure 18) that is necessary to calculate the volume resistivity, a Leica DM2500 M microscope with an incorporated camera was used. The multifilaments diameter was considered as cylindrical.

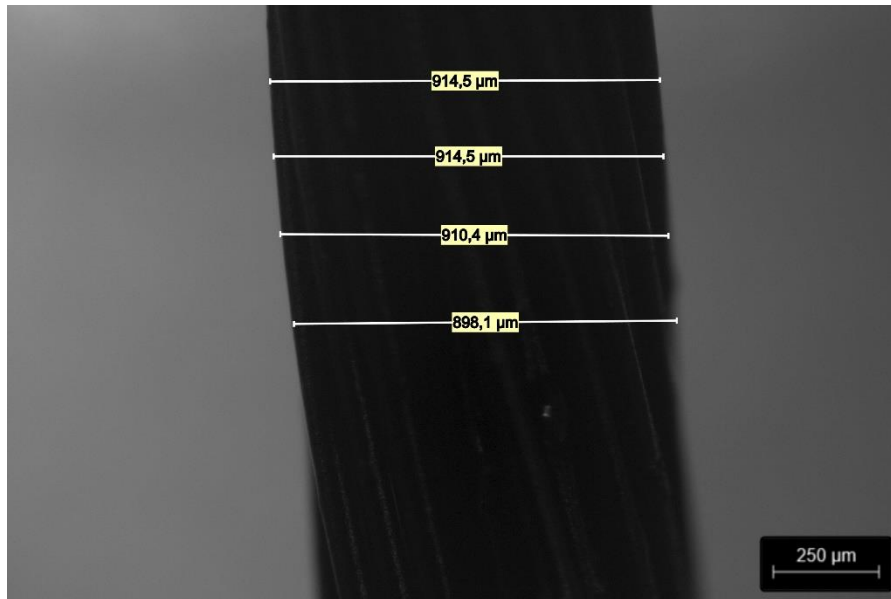


Figure 18 - Representative image of the measurement of the longitudinal cross-section geometry of the multifilaments.

9.2 Mechanical characterization

The mechanical characterization was carried out in a universal mechanical testing machine, model AGXV-50kN from Shimadzu, to determine the mechanical properties of the multifilaments, following the ASTM 3822:07 standard. The length between the rubber coated grips was 25 mm, the tensile test speed was 250 mm/min, and a load cell of 100 N was used. The main mechanical properties, elongation at break (%) and tenacity (cN/dtex), were studied. Elongation at break corresponds to the increase in length of the test specimen compared to its starting length (expressed in %), while applying a deformation at the indicated speed. Tenacity is described as the specific stress corresponding to the maximum force in a stress-strain curve. For this result, it is important to consider the linear density of the multifilaments in calculating tenacity, since each multifilament can have a different linear density and diameter [66].

For each fiber, at least, 12 samples were tested in standard atmosphere conditions (room temperature: $25,5 \pm 0,05$ °C; relative humidity: $60,0 \pm 0,05$ %).

Prior to the tensile tests, the linear density of each fiber was measured. The linear density, whose unit is decitex (dtex), corresponds to the weight in grams per 10000 meters of multifilament. These measurements were performed in a wrap reel test model 161M from Mesdan.

9.3 Joule heating tests for multifilaments

The Joule heating tests of the multifilaments was conducted in an identical way as for the nanocomposites.

The setup for this characterization consisted in an acrylic part (Figure 19 a)) with two sides covered with copper tape. Then, the multifilament was rolled around this acrylic part (Figure 19 b)) and the highly conductive silver ink was applied to the zones of the multifilament that were in contact with the copper tape. Then, the silver ink was cured in an oven at 120 °C for 20 minutes and, lastly, the multifilaments were again covered with copper tape.

The measurements were carried out using a power source connected to two ends of the copper tape and three test of 5 minutes each were carried out applying three different voltages (12V, 24V and 48V). A FLIR A700 thermal camera was used to record the temperature variations of the multifilaments and, finally, the results were examined in the FLIR Tools software.

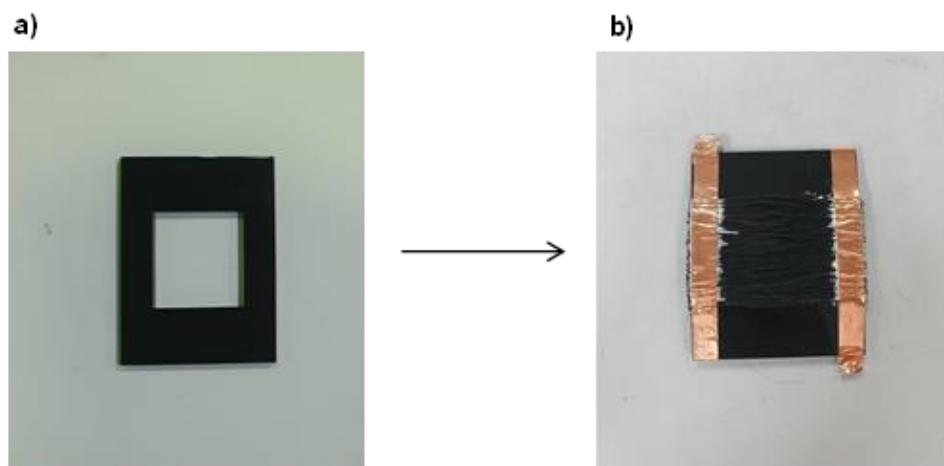


Figure 19 – Setup used for the thermal characterization of the multifilaments: **a)** acrylic part and **b)** final setup.

IV. Results and Discussion

10. Characterization of PBT/CNTs nanocomposites

10.1 Study of the electrical percolation threshold

The values of electrical conductivity of the PBT/MWCNTs are presented in Figure 20 and it shows that the incorporation of MWCNTs significantly increased the electrical conductivity of the nanocomposites.

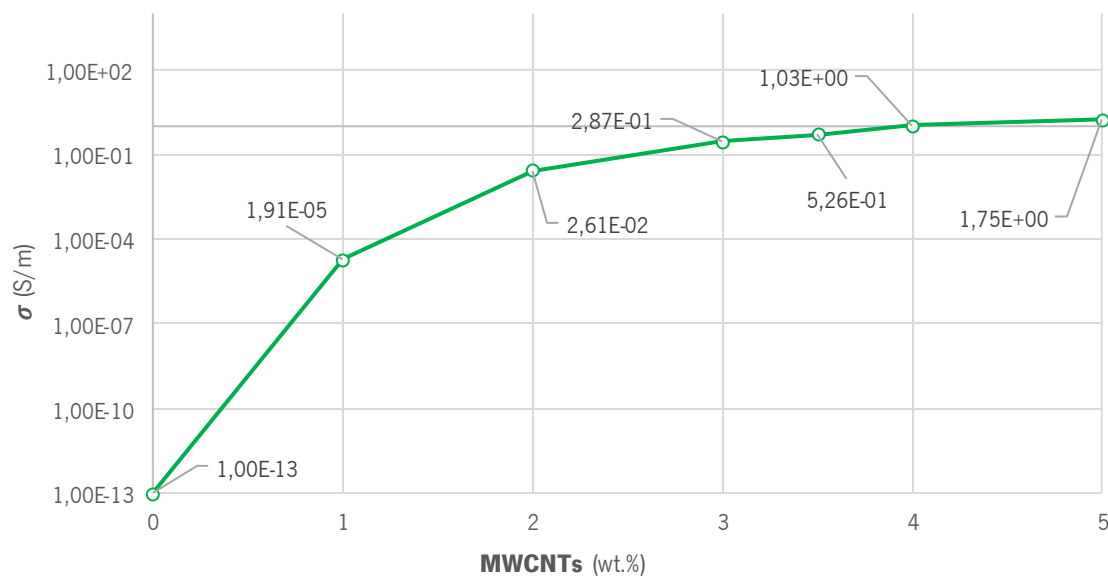


Figure 20 – Electrical conductivity as a function of MWCNTs concentration.

The value of electrical conductivity of neat PBT is 1×10^{-13} S/m. The electrical percolation threshold occurred between 0 wt.% and 1wt.% with an increment from 1×10^{-13} to $1,91 \times 10^{-5}$ S/m. The maximum value of electrical conductivity was 1,75 S/m with a filler content of 5 wt.%.

With the addition of a small filler content of MWCNTs it was possible to obtain a transition from an insulating to a semiconductor material, with the electrical conductivity increasing approximately 8 orders of magnitude relative to the raw polymer. The addition of MWCNTs to the PBT matrix caused an increase of the electrical conductivity by creating a continuous network of contacts between the MWCNTs.

10.2 Heating evaluation

The heating test was carried out in order to evaluate the heat dissipation in the nanocomposites when submitted to different voltages. The results of these test are presented in Figure 21 and only the PBT/3%CNTs was characterized since was not possible to create a setup with a low enough resistance with the other nanocomposites (PBT with 1 and 2 wt.% of MWCNTs). Previously, a target temperature was established between 35 and 40 °C and the time that took to reach that temperature was also obtained with the FLIR Tools software as well as the maximum temperature reached by the setup (Table 10).

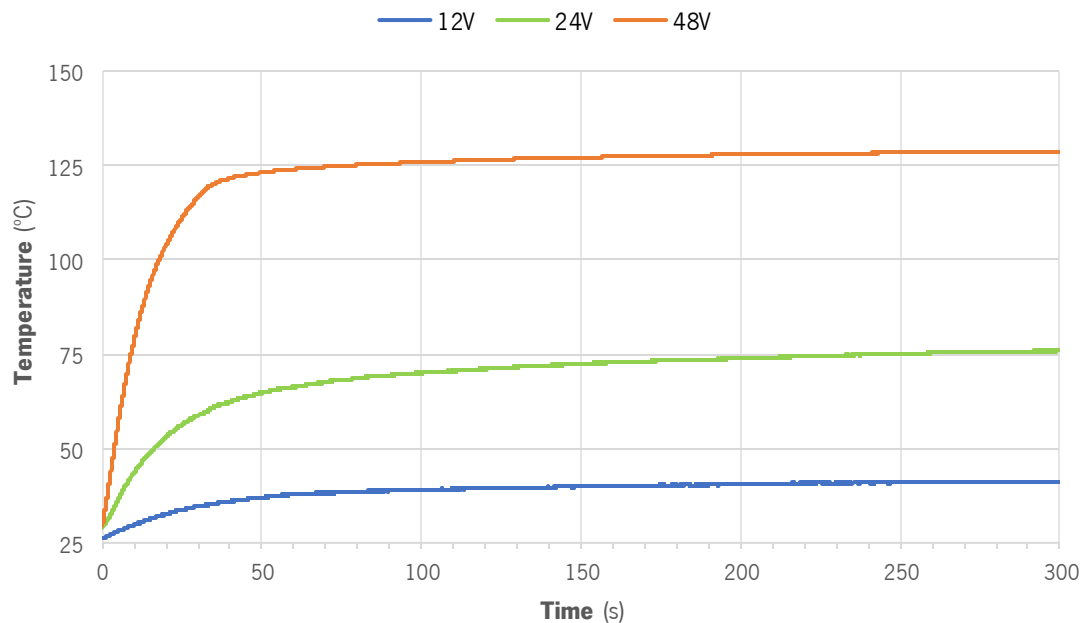


Figure 21 – Temperature variation over time during the Joule heating tests for the PBT/3%CNTs.

Table 10 – Maximum temperature and time taken to reach the target temperature in each test.

Test	Maximum Temperature (°C)	Time to reach 40 °C (s)
12 V	41,2	120
24 V	75,9	7
48 V	128,7	2

As it is possible to observe in Figure 21, with a voltage of 12 V, the nanocomposites were able to reach the target temperature established previously in 120 s. The tests performed with 24 V and 48 V demonstrate that the nanocomposites quickly heat up to 40 °C (7 and 2 seconds, respectively) and, after this, achieve a plateau stage at a higher temperature.

As described in chapter II, it was observed that the nanocomposites presented the Joule heating effect, since the applied electrical current to the nanocomposites was converted to dissipated heat.

10.3 Melt flow index

The MFI measurements were performed in order to evaluate the spinnability of the nanocomposite as well as to study the influence of the MWCNTs on the PBT viscosity. The results are presented in Figure 22.

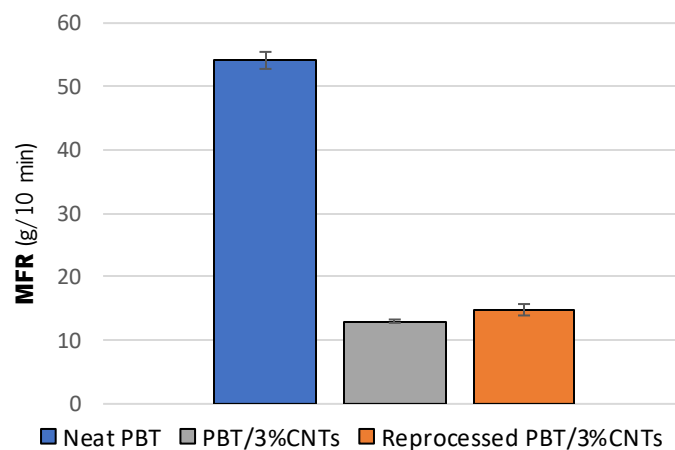


Figure 22 – Comparison between melt flow rate values of the neat polymer and the nanocomposite.

The PBT/3%CNTs was tested in order to study the effect of a second processing in the melt flow rate values and because it was the only composite capable of heating up by Joule effect, as will be discussed in the next subchapter. The results show that the melt flow rate decreases when the MWCNTs are added to the PBT matrix reaching values of 13 g/10min and 15,8 g/10min for PBT/3%CNTs and reprocessed PBT/3%CNTs, respectively, showing that the composites are within the operating window of the multifilament production equipment. Thus, these melt flow rate values are acceptable for the melt-spinning technique.

10.4 Macrodispersion

The optical microscopy was employed to study the presence of agglomerates in the PBT/3%CNTs nanocomposite. Figure 23 displays representative images of the nanocomposite obtained during the morphological analysis.

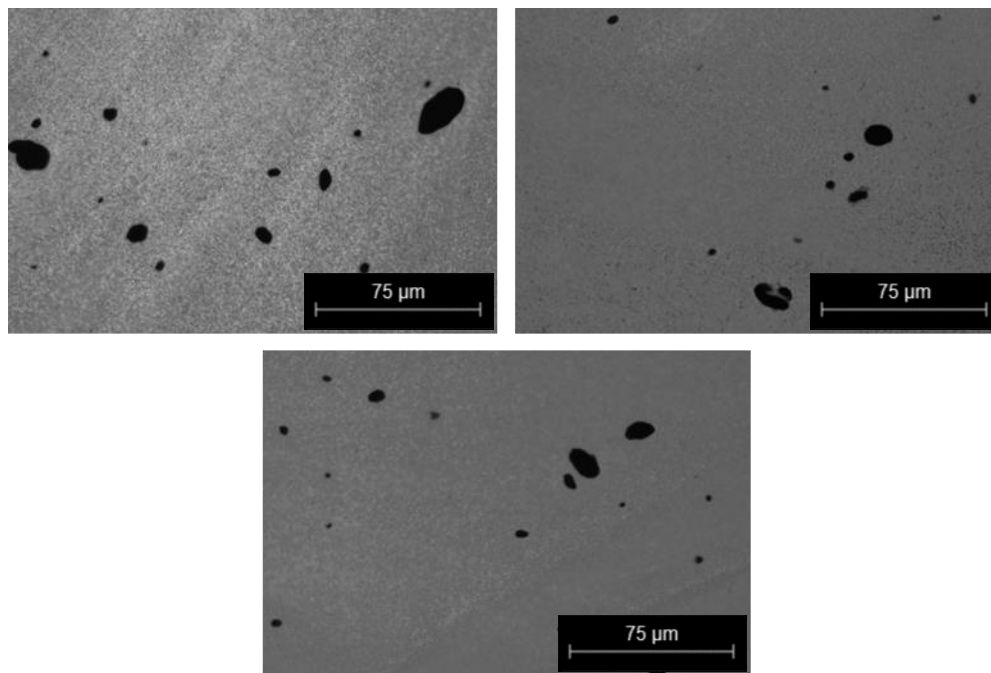


Figure 23 – Images obtained with OM of the PBT/3% nanocomposite (magnification 20x).

By analyzing the images, it is possible to observe some agglomerates with different sizes. Therefore, a quantitative analysis was performed in order to examine the distribution of the agglomerate areas and the results are represented in the histogram in Figure 24. The area distribution of the agglomerates is obtained by the number of agglomerates (normalized per mm^2) versus the different agglomerates area classes (each class corresponds to $250 \mu\text{m}^2$).

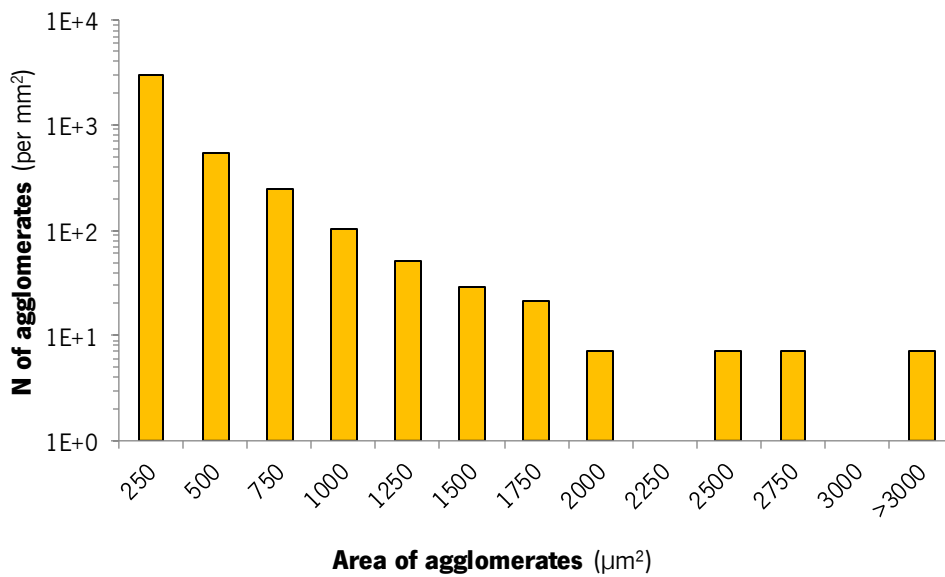


Figure 24 – Number of agglomerates (per mm²) as a function of the area of agglomerates of the PBT/3%CNTs nanocomposite.

When analyzing Figure 24, it is noticeable that the majority of agglomerates are represented in the first area classes (smaller agglomerate areas) which can be problematic to the melt-spinning technique. The presence of a few larger agglomerates is also observed, which could mean that the nanocomposite is reaching a saturation level and is no longer able to disperse individual MWCNTs into the bulk composite. This was expectable since 3 wt.% of MWCNTs is already above the percolation threshold (between 0 and 1 wt.%) which can lead to an excessive concentration of MWCNTs and, consequently, the formation of larger agglomerates.

11. Influence of graphite addition

11.1 Electrical conductivity

The results obtained for the electrical conductivity of the hybrid composites are presented in Figure 25 and it displays the effect of the addition of graphite to the PBT with 2 wt.% of MWCNTs nanocomposites. The selection of this nanocomposite was based on the fact that it was expected that the electrical conductivity of the multifilaments would decrease when compared to the nanocomposite rods [44].

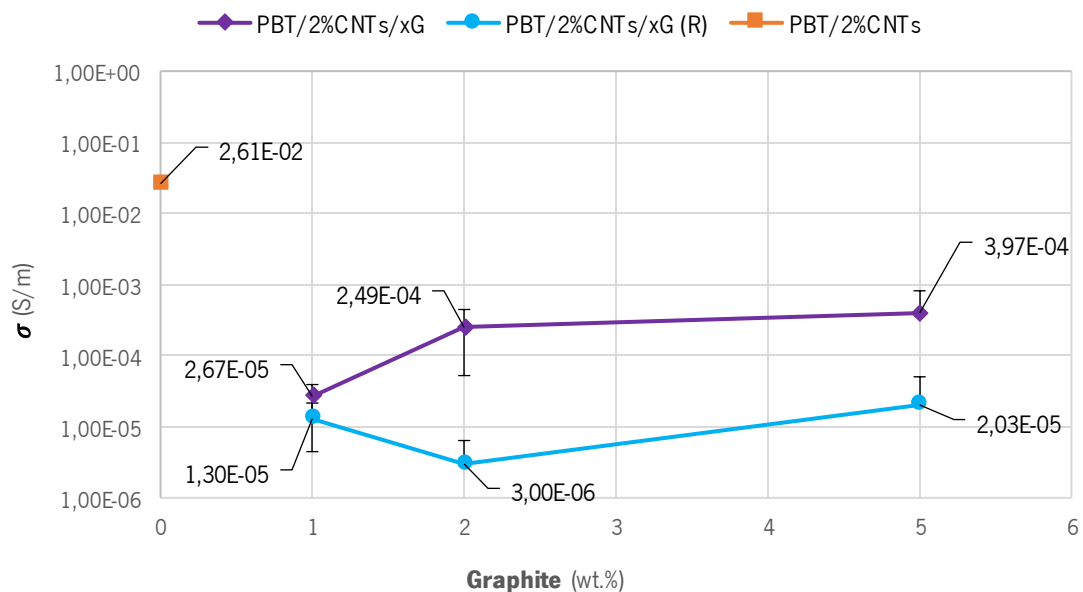


Figure 25 – Electrical conductivity as a function of graphite concentration (purple line represents the ternary nanocomposites with 1 processing; blue line represents the hybrid nanocomposites with 2 processing steps).

When compared to the electrical conductivity of the PBT with 2 wt.% of MWCNTs (Figure 20), it is observed that the addition of graphite had a negative impact on the electrical conductivity, decreasing it by 3 orders of magnitude (from $2,61 \times 10^{-2}$ to $2,67 \times 10^{-5}$ S/m) for the hybrid composites (purple line) and 4 orders of magnitude (from $2,61 \times 10^{-2}$ to $3,00 \times 10^{-6}$ S/m) for the reprocessed hybrid composites (blue line). It was expected that the addition of graphite could increase the electrical conductivity of the PBT with 2 wt.% of MWCNTs nanocomposite (or at least not decrease it), since it is expected that graphene sheets help dispersing the MWCNTs, separating the entangled nanotubes, and forming an effective conductive pathway, as Liu *et al.* reported [67].

Conversely, Joseph *et al.* [68] concluded that this synergy between graphene sheets and carbon nanotubes is only achievable when using concentrations below the percolation threshold, since above this value, a decrease of the electrical conductivity is verified. Therefore, the results presented in Figure 25 are not in line with the previous studies probably because the filler content of MWCNTs was above the electrical percolation threshold.

11.2 Macrodispersion

The morphological analysis was conducted to evaluate the presence of agglomerates in the ternary composites. The images in Figure 26 correspond to the cross-section of the hybrid nanocomposites obtained by OM.

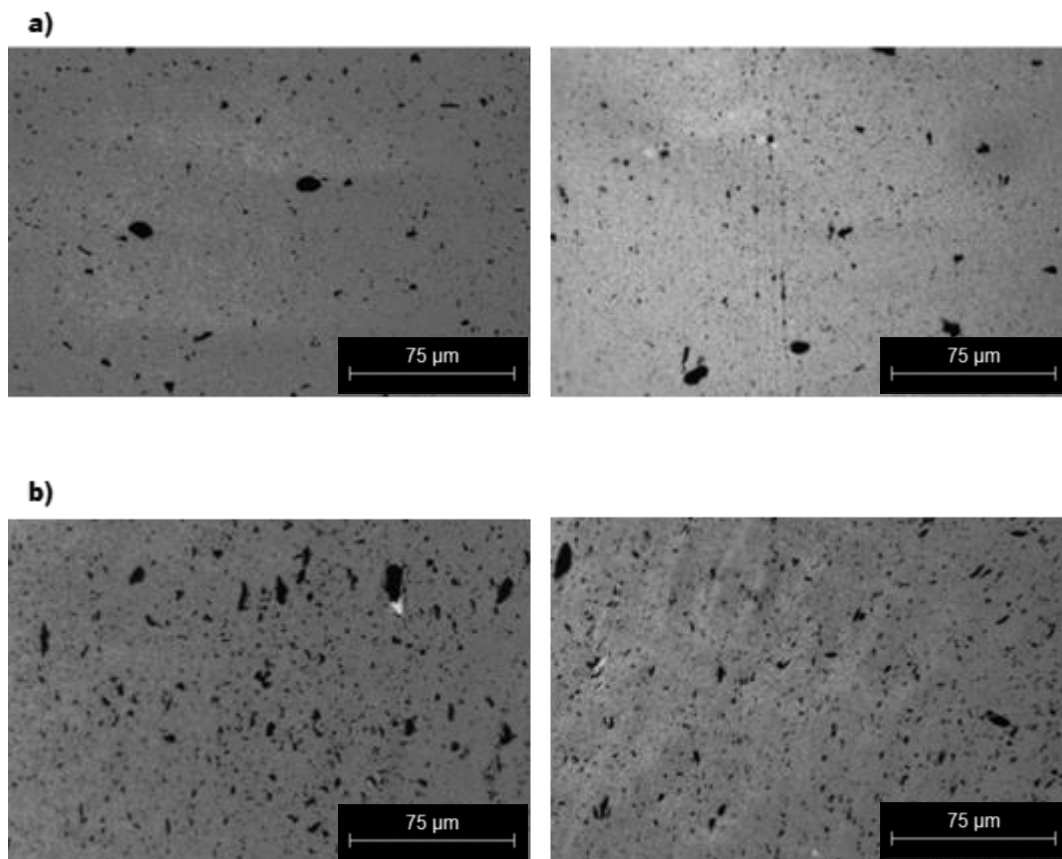


Figure 26 – Representative images obtain by OM of the ternary nanocomposites (magnification 20x): a) PBT/2%CNTs/1%G; b) PBT/2%CNTs/5%G.

Figure 26 presents the cross-section of the samples studied in this work, which were the PBT with 3 wt.% of carbon nanoparticles (2 wt.% of MWCNTs and 1wt.% of graphite – a)) and with

7 wt.% of carbon nanoparticles (2 wt.% of MWCNTs and 5 wt.% of graphite – b)). When compared to the PBT/3%CNTs nanocomposites (Figure 24), an increase of the smaller size agglomerates is observed, as a consequence of the addition of graphite. This is evidenced by the histograms in Figure 27.

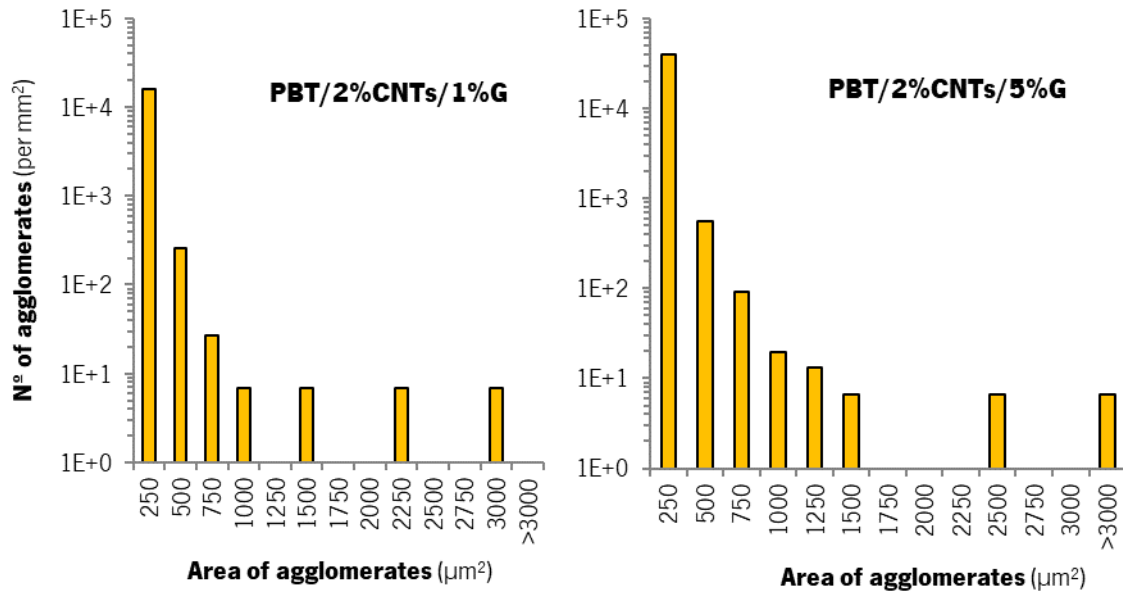


Figure 27 – Number of agglomerates (per mm²) as a function of the agglomerate areas of the analyzed hybrid nanocomposites.

These results show the addition of graphite increased the number of smaller size particles, from the PBT/2%CNTs/1%G to the PBT/2%CNTs/5%G. As stated earlier in chapter V, the hybrid nanocomposites have a MWCNTs concentration over the percolation threshold because of the expected loss of electrical conductivity in the multifilaments. Despite the negative effect of the graphite addition, it is observed that it helped reducing the average size of the agglomerates which is advantageous for the production of multifilaments. Therefore, the graphite helped the dispersion of the agglomerates but increased the number of smaller size particles.

12. Multifilaments characterization

12.1 Electrical conductivity

The influence of the different processing conditions (pump speed and temperature of roll 2) (Table 11) on the electrical conductivity results of the multifilaments are presented in Figure 28. OS_x is the designation used for each multifilament fiber produced. OS_1 was produced with neat PBT and OS_2 to OS_7 with PBT/3%CNTs.

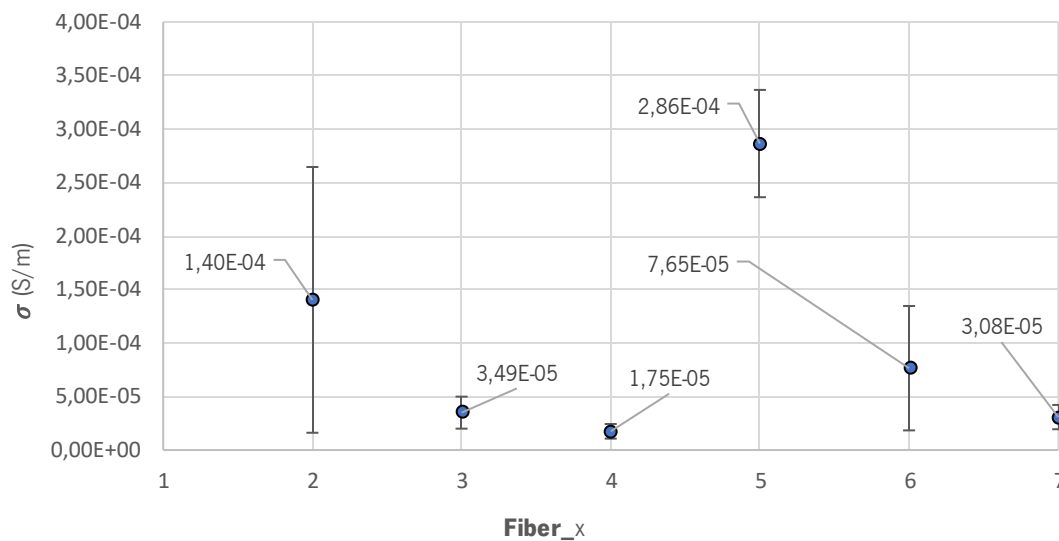


Figure 28 – Electrical conductivity of each multifilament fiber produced.

Considering the processing conditions that have been studied, it is possible to observe that the lower pump speeds (10 rpm) favor the electrical conductivity, since OS_2 and OS_5 ($1,4 \times 10^{-4}$ and $2,86 \times 10^{-4}$ S/m, respectively) have the best results when compared to the other fibers processed with the same conditions. This is verified since the higher pump speed induces higher shear rates and this leads to the destruction of the conductive network and, consequently, a decrease of the electrical conductivity, as stated in [69]. It is also noticeable that the increase of the temperature of roll 2 (from 40 to 55 °C) had a minor influence in the conductivity values as OS_5, OS_6 and OS_7 ($2,86 \times 10^{-4}$, $7,65 \times 10^{-5}$, and $3,08 \times 10^{-5}$ S/m) present just slightly higher electrical conductivity when compared to OS_2, OS_3 and OS_4 ($1,4 \times 10^{-4}$, $3,49 \times 10^{-5}$, and $1,75 \times 10^{-5}$ S/m), respectively.

A decrease of 3 to 4 orders of magnitude of the electrical conductivity is observed from the nanocomposite ($2,87 \times 10^{-1}$ S/m) to the multifilaments ($2,86 \times 10^{-4}$ S/m) which was expected

because of the lower diameter of the multifilaments compared to the nanocomposite rods and the effect of drawing between the spinneret and roll 1 which induce orientation and increase the distance between the nanoparticles. Despite this decrease, these results are still satisfactory since other studies, like Bouchard *et al.* [44], experienced a decrease of 10 orders of magnitude from the melt compounded composite to the melt-spun fibers which is a much greater drop than the one presented above.

Table 11 – Process conditions of the multifilaments.

Sample	Material	Rolls Speed (R1; R2; R3) (m/min)	Rolls Temperature (R1; R2) (°C)	DDR	CDR	Pump Speed (rpm)	Feed rate (g/min)	Pressure at spinneret (bar)
Fiber_1	Neat PBT	150;350;350	60;40	52	2,3	10	32,12	47
Fiber_2	PBT/3%CNTs	100;100;100	60:40	35	1	10	32,12	98
Fiber_3	PBT/3%CNTs	100;100;100	60:40	25	1	14	44,97	120
Fiber_4	PBT/3%CNTs	100;100;100	60:40	20	1	18	57,82	133
Fiber_5	PBT/3%CNTs	100;100;100	60:55	35	1	10	32,12	93
Fiber_6	PBT/3%CNTs	100;100;100	60:55	25	1	14	44,97	116
Fiber_7	PBT/3%CNTs	100;100;100	60:55	20	1	18	57,82	135

12.2 Mechanical characterization

The results of the tensile tests of the multifilaments are presented in Figure 29. With these tests, it is possible to analyze the elongation at break and the tenacity of the fibers.

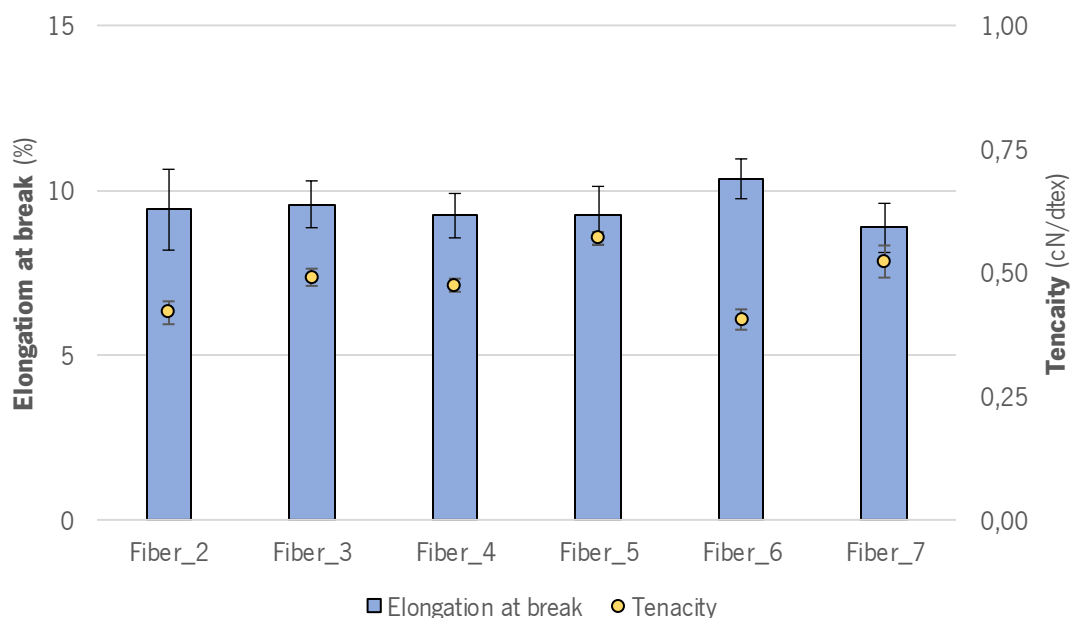


Figure 29 – Elongation at break and tenacity results for the fibers produced under each set of conditions.

It was observed that neither the elongation at break or the tenacity vary significantly with the different processing conditions used since the elongation at break values are approximately 10 % and the tenacity is comprised between 0,41 and 0,57 cN/dtex.

However, it is interesting to note that the elongation at break and the tenacity decreases substantially when compared to the pure PBT fibers that show an elongation at break of 260 % and a tenacity of 1,16 cN/dtex. This indicates that the addition of MWCNTs reduced the mechanical properties and, consequently, the conductive particles had no obvious reinforcing effect on the PBT matrix. The presence of agglomerates of rigid nanoparticles may lead to an effect within the matrix similar to the appearance of voids or weak points in the contact between the matrix and the nanoparticles. Therefore, the decrease of the elongation at break was expected because of the addition of rigid particles. However, the decrease of tenacity may occur due to a bad PBT/nanoparticle interface.

12.3 Heating evaluation

The Joule heating tests of the multifilaments was carried out by performing similar tests as those for the nanocomposites. The results are presented in Figure 30.

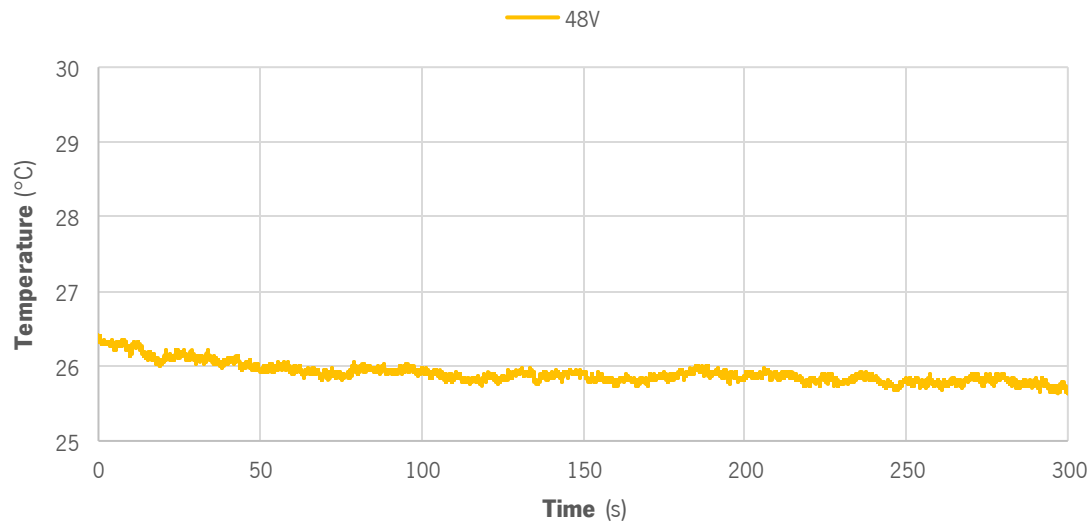


Figure 30 – Temperature variation over time during the Joule heating tests for the multifilaments.

Only one test was carried out with a voltage of 48 V, and the temperature of the multifilaments remained constant throughout the test. The multifilaments used in this characterization were from OS_2 ($2,86 \times 10^{-4}$ S/m). However, the overall resistance of the setup used was $2,1 \times 10^6 \Omega$. The result showed that the Joule effect was not relevant in the multifilaments, which indicated that the electrical conductivity is not high enough to promote the heating of the fibers. Also, this result for the thermal dissipation can be due to the reduction of diameter of the multifilaments as compared to the nanocomposites, as well as the setup used, that could lead to a bad contact between all the multifilaments despite the efforts to compact them using the copper tape.

V. Conclusions

The main objective of this work was the production of multifilaments with heating conduction properties by the melt-spinning technology.

The Joule heating tests were performed with the objective of checking the nanocomposites response for heating as induced by an electric current. The results of these tests showed that the PBT/3%CNTs nanocomposite can heat up when submitted to an electric current proving the possibility of applying the Joule heating effect. This nanocomposite reached a temperature of 41,2 °C in 5 minute in a test where a voltage of 12 V was applied. This test was the most important for the selection of the nanocomposite that would be used for the production of multifilaments which, ultimately, demonstrated that the PBT/3%CNTs composites were adequate for the application, despite of the expected decrease of the electrical conductivity in the melt-spinning technique.

After the selection of the polymer matrix and the conductive filler, the nanocomposites preparation was divided into 2 steps. Firstly, a study of the electrical percolation threshold was conducted by melt compounding and characterization the PBT/CNTs nanocomposites with the following filler contents: 5; 4; 3,5; 3; 2 and 1 wt.%. The electrical characterization showed an increase of the electrical conductivity by 8 orders of magnitude from the raw polymer (1×10^{-13} S/m) to the PBT with 1 wt.% of MWCNTs nanocomposite ($2,11 \times 10^{-5}$ S/m), meaning that the electrical percolation threshold is below 1 wt.% of MWCNTs. Afterwards, based on these results, the PBT with 2wt.% of MWCNTs was selected to combine with graphite to produce the hybrid nanocomposites with concentrations of 1, 2 and 5 wt.% of graphite. Then, another electrical characterization was performed with this hybrid composites to examine the effect of the addition of graphite. It was observed that the graphite did not enhance the electrical conductivity comparatively to the PBT/CNTs nanocomposites decreasing the value from 2 ($4,85 \times 10^{-4}$ S/m) to 4 ($3,41 \times 10^{-6}$ S/m) orders of magnitude. Therefore, it was observed that the addition of the conductive fillers increased the electrical conductivity of the PBT matrix, but no synergistic effect was observed with graphite since a filler content of MWCNTs above the electrical percolation threshold was used in the hybrid nanocomposites.

The morphological analysis was carried out with the purpose to evaluate the presence of agglomerates in the nanocomposites. The increase of smaller sized agglomerates ($< 1000 \mu\text{m}^2$) in the hybrid nanocomposites is related to the large content of graphite nanoflakes, and it is

possible that these composites are reaching a saturation level for the MWCNTs dispersion in the PBT bulk. The same was observed for the PBT/3%CNTs morphological analysis since the presence of relatively large agglomerates was observed.

Finally, after all the characterization tests of the nanocomposites, the production of the multifilaments was carried out. Six different multifilaments were produced by varying the pump speed and the temperature of the second roll. These two variables showed that the lower pump speed favored the electrical conductivity, reaching the highest values ($1,4 \times 10^{-4}$ and $2,86 \times 10^{-4}$ S/m). Also, comparatively to the values of electrical conductivity of the nanocomposites, the electrical conductivity of the multifilaments decreased 3 and 4 orders of magnitude which is a very satisfactory result, when compared to the literature review. On the other hand, the mechanical characterization showed that the MWCNTs did not have an obvious reinforcement effect in the PBT composite. To conclude, the Joule heating tests of the multifilaments demonstrated that the fibers produced could not heat up when submitted to an electrical current, despite carrying out a test where a voltage of 48 V was applied.

13. Proposal for future work

With the purpose of obtaining composites with improved electrical properties it is suggested that the melt compounding conditions of the nanocomposites should be analyzed in order to optimize them to reduce the presence of agglomerates and enhance the electrical conductivity. Another possibility is to functionalize the CNTs to promote a better dispersion and adhesion to PBT. The thermogravimetric tests would be useful in order to evaluate the real percentage of nanoparticles incorporated in the polymer matrix as well as transmission electron microscopy (TEM) or scanning electron microscopy (SEM) to observe the individual dispersion state and interface of the carbon nanoparticles in the polymer matrix.

For the multifilaments characterization it is recommended to build a setup for the heating tests specifically to study the Joule heating effect, to enhance the multifilament contact and heat/current transmission, since the characterization performed in this work was not able to obtain satisfactory results.

IV. Bibliography

- [1] N. Mohd Nurazzi, A. Khalina, S. M. Sapuan, A. H. A. M. Dayang Laila, M. Rahmah, and Z. Hanafee, "A review: Fibres, polymer matrices and composites," *Pertanika J. Sci. Technol.*, vol. 25, no. 4, pp. 1085–1102, 2017.
- [2] Z. Han and A. Fina, "Thermal conductivity of carbon nanotubes and their polymer nanocomposites: A review," *Prog. Polym. Sci.*, vol. 36, no. 7, pp. 914–944, 2011, doi: 10.1016/j.progpolymsci.2010.11.004.
- [3] J. Che, K. Wu, Y. Lin, K. Wang, and Q. Fu, "Largely improved thermal conductivity of HDPE/expanded graphite/carbon nanotubes ternary composites via filler network-network synergy," *Compos. Part A Appl. Sci. Manuf.*, vol. 99, pp. 32–40, 2017, doi: 10.1016/j.compositesa.2017.04.001.
- [4] M. A. Al Faruque, A. Kiziltas, D. Mielewski, and M. Naebe, "A facile approach of fabricating electrically conductive knitted fabrics using graphene oxide and textile-based waste material," *Polymers (Basel)*, vol. 13, no. 17, 2021, doi: 10.3390/polym13173003.
- [5] J. R. Bautista-Quijano, P. Pötschke, H. Brünig, and G. Heinrich, "Strain sensing, electrical and mechanical properties of polycarbonate/multiwall carbon nanotube monofilament fibers fabricated by melt spinning," *Polymer (Guildf)*, vol. 82, pp. 181–189, 2016, doi: 10.1016/j.polymer.2015.11.030.
- [6] S. J. Park and M. K. Seo, *Types of Composites*, vol. 18. 2011.
- [7] Ricardo Rodrigo Ramos Cecci, Adriano Alves Passos, Nathan Riany Valério Albino, Daniel da Silva Vicente, Ademir Severino Duarte, and Maria Inês Bruno Tavares, "Effect of Graphene Nanoplatelets Presence on the Thermal and Mechanical Properties of Polypropylene Fibers Produced by Melt Spinning," *J. Mater. Sci. Eng. B*, vol. 10, no. 2, 2020, doi: 10.17265/2161-6221/2020.3-4.002.
- [8] B. Yang *et al.*, "Melt crystallization and thermal properties of graphene platelets (GNPs) modified recycled polyethylene terephthalate (RPET) composites: The filler network analysis," *Polym. Test.*, vol. 77, no. January, p. 105869, 2019, doi: 10.1016/j.polymertesting.2019.04.016.
- [9] U. Szeluga, B. Kumanek, and B. Trzebicka, "Synergy in hybrid polymer/nanocarbon composites. A review," *Compos. Part A Appl. Sci. Manuf.*, vol. 73, pp. 204–231, 2015,

- doi: 10.1016/j.compositesa.2015.02.021.
- [10] S. Kumar *et al.*, "Study on mechanical, morphological and electrical properties of carbon nanofiber/polyetherimide composites," *Mater. Sci. Eng. B Solid-State Mater. Adv. Technol.*, vol. 141, no. 1–2, pp. 61–70, 2007, doi: 10.1016/j.mseb.2007.06.002.
- [11] P. C. Ma, N. A. Siddiqui, G. Marom, and J. K. Kim, "Dispersion and functionalization of carbon nanotubes for polymer-based nanocomposites: A review," *Compos. Part A Appl. Sci. Manuf.*, vol. 41, no. 10, pp. 1345–1367, 2010, doi: 10.1016/j.compositesa.2010.07.003.
- [12] A. Cayla, C. Campagne, M. Rochery, and E. Devaux, "Melt spun multifilament yarns of carbon nanotubes-based polymeric blends: Electrical, mechanical and thermal properties," *Synth. Met.*, vol. 162, no. 9–10, pp. 759–767, 2012, doi: 10.1016/j.synthmet.2012.03.021.
- [13] M. A. Kashfipour, N. Mehra, and J. Zhu, "A review on the role of interface in mechanical, thermal, and electrical properties of polymer composites," *Adv. Compos. Hybrid Mater.*, vol. 1, no. 3, pp. 415–439, 2018, doi: 10.1007/s42114-018-0022-9.
- [14] H. Chen *et al.*, "Thermal conductivity of polymer-based composites: Fundamentals and applications," *Prog. Polym. Sci.*, vol. 59, pp. 41–85, 2016, doi: 10.1016/j.progpolymsci.2016.03.001.
- [15] H. P. L. Martins, "Filamentos condutores baseados em compósitos com nanopartículas de carbono," 2017.
- [16] C. Feng, D. Zhu, Y. Wang, and S. Jin, "Electromechanical behaviors of graphene reinforced polymer composites: A review," *Materials (Basel)*, vol. 13, no. 3, 2020, doi: 10.3390/ma13030528.
- [17] J. Grothe, S. Kaskel, and A. Leuteritz, *Nanocomposites and Hybrid Materials*, vol. 1–10. Elsevier B.V., 2012.
- [18] A. V. Rane, K. Kanny, V. K. Abitha, S. Thomas, and S. Thomas, *Methods for Synthesis of Nanoparticles and Fabrication of Nanocomposites*. Elsevier Ltd., 2018.
- [19] D. Verma and K. L. Goh, *Functionalized Graphene-Based Nanocomposites for Energy Applications*. Elsevier Inc., 2019.
- [20] M. Solazzo, F. J. O'Brien, V. Nicolosi, and M. G. Monaghan, "The rationale and emergence of electroconductive biomaterial scaffolds in cardiac tissue engineering," *APL Bioeng.*, vol. 3, no. 4, 2019, doi: 10.1063/1.5116579.

- [21] F. Giubileo, A. Di Bartolomeo, L. Lemmo, G. Luongo, and F. Urban, "Field emission from carbon nanostructures," *Appl. Sci.*, vol. 8, no. 4, pp. 1–21, 2018, doi: 10.3390/app8040526.
- [22] Z. Yenier, S. Aker, Y. Seki, L. Altay, O. Bigun, and M. Sarikanat, "Improving thermal conductivity of polybutylene terephthalate composites with hybrid synthetic graphite and carbon fiber," *J. Thermoplast. Compos. Mater.*, 2021, doi: 10.1177/08927057211018491.
- [23] A. A. Tarhini and A. R. Tehrani-Bagha, "Graphene-based Polymer Composite Films with Enhanced Mechanical Properties and Ultra-high In-plane Thermal Conductivity," *Compos. Sci. Technol.*, vol. 184, no. July 2019, p. 107797, 2019, doi: 10.1016/j.compscitech.2019.107797.
- [24] D. E. S. de Sousa, C. H. Scuracchio, G. M. de Oliveira Barra, and A. de Almeida Lucas, *Expanded graphite as a multifunctional filler for polymer nanocomposites*. Elsevier Inc., 2015.
- [25] J. Zavickis, A. Linarts, and M. Knite, "The downshift of the electrical percolation threshold in polyisoprene-nanostructured carbon composites," *Energetika*, vol. 8, no. 1, pp. 44–49, 2011, doi: 10.6001/energetika.v57i1.2043.
- [26] M. K. Seo, J. R. Lee, and S. J. Park, "Crystallization kinetics and interfacial behaviors of polypropylene composites reinforced with multi-walled carbon nanotubes," *Mater. Sci. Eng. A*, vol. 404, no. 1–2, pp. 79–84, 2005, doi: 10.1016/j.msea.2005.05.065.
- [27] Q. Zhang, S. Rastogi, D. Chen, D. Lippits, and P. J. Lemstra, "Low percolation threshold in single-walled carbon nanotube/high density polyethylene composites prepared by melt processing technique," *Carbon N. Y.*, vol. 44, no. 4, pp. 778–785, 2006, doi: 10.1016/j.carbon.2005.09.039.
- [28] G. Hu, C. Zhao, S. Zhang, M. Yang, and Z. Wang, "Low percolation thresholds of electrical conductivity and rheology in poly(ethylene terephthalate) through the networks of multi-walled carbon nanotubes," *Polymer (Guildf.)*, vol. 47, no. 1, pp. 480–488, 2006, doi: 10.1016/j.polymer.2005.11.028.
- [29] A. Allaoui, S. Bai, H. M. Cheng, and J. B. Bai, "Mechanical and electrical properties of a MWNT/epoxy composite," vol. 62, pp. 1993–1998, 2002.
- [30] A. Dorigato, V. Freitas, J. A. Covas, M. C. Paiva, M. Brugnara, and A. Pegoretti, "Evaluation of the role of carbon nanotubes on the electrical properties of poly(butylene

- terephthalate) nanocomposites for industrial applications,” *J. Elastomers Plast.*, vol. 51, no. 1, pp. 3–25, 2019, doi: 10.1177/0095244318768634.
- [31] A. Dorigato, M. Brugnara, and A. Pegoretti, “Synergistic effects of carbon black and carbon nanotubes on the electrical resistivity of poly(butylene-terephthalate) nanocomposites,” *Adv. Polym. Technol.*, vol. 37, no. 6, pp. 1744–1754, 2018, doi: 10.1002/adv.21833.
- [32] S. G. Prolongo, R. Moriche, G. Del Rosario, A. Jiménez-Suárez, M. G. Prolongo, and A. Ureña, “Joule effect self-heating of epoxy composites reinforced with graphitic nanofillers,” *J. Polym. Res.*, vol. 23, no. 9, 2016, doi: 10.1007/s10965-016-1092-4.
- [33] H. Chu, Z. Zhang, Y. Liu, and J. Leng, “Self-heating fiber reinforced polymer composite using meso/macropore carbon nanotube paper and its application in deicing,” *Carbon N. Y.*, vol. 66, pp. 154–163, 2014, doi: 10.1016/j.carbon.2013.08.053.
- [34] B. Mas, J. P. Fernández-Blázquez, J. Duval, H. Bunyan, and J. J. Vilatela, “Thermoset curing through Joule heating of nanocarbons for composite manufacture, repair and soldering,” *Carbon N. Y.*, vol. 63, pp. 523–529, 2013, doi: 10.1016/j.carbon.2013.07.029.
- [35] J. Orellana, I. Moreno-villoslada, R. K. Bose, F. Picchioni, M. E. Flores, and R. Araya-hermosilla, “Self-healing polymer nanocomposite materials by joule effect,” *Polymers (Basel)*, vol. 13, no. 4, pp. 1–24, 2021, doi: 10.3390/polym13040649.
- [36] U. K. Sanivada, D. Esteves, L. M. Arruda, C. A. Silva, I. P. Moreira, and R. Figueiro, “Joule-Heating Effect of Thin Films with Carbon-Based Nanomaterials,” *Materials (Basel)*, vol. 15, no. 12, 2022, doi: 10.3390/ma15124323.
- [37] J. A. Covas and M. C. Paiva, “Monitoring Dispersion and Re-agglomeration Phenomena During the Manufacture of Polymer Nanocomposites,” *Process. Polym. Nanocomposites*, pp. 97–120, 2019, doi: 10.3139/9781569906361.003.
- [38] G. R. Kasaliwal, T. Villmow, S. Pegel, and P. Pötschke, *Influence of material and processing parameters on carbon nanotube dispersion in polymer melts*. Woodhead Publishing Limited, 2011.
- [39] S. A. Ashter, *Other Processing Approaches*. 2014.
- [40] P. Pötschke, S. M. Dudkin, and I. Alig, “Dielectric spectroscopy on melt processed polycarbonate - Multiwalled carbon nanotube composites,” *Polymer (Guildf)*, vol. 44, no. 17, pp. 5023–5030, 2003, doi: 10.1016/S0032-3861(03)00451-8.

- [41] G. R. Kasaliwal, "Influence of Processing Conditions in Small-Scale Melt Mixing and Compression Molding on the Resistivity and Morphology of Polycarbonate-MWNT Composites," *J. Appl. Polym. Sci.*, vol. 116, no. 5, pp. 2658–2667, 2010, doi: 10.1002/app.
- [42] R. Hufenus, Y. Yan, M. Dauner, and T. Kikutani, "Melt-spun fibers for textile applications," *Materials (Basel)*, vol. 13, no. 19, pp. 1–32, 2020, doi: 10.3390/ma13194298.
- [43] C. Lawrence, *Fibre to Yarn: Filament Yarn Spinning*. Elsevier Ltd, 2014.
- [44] J. Bouchard, A. Cayla, V. Lutz, C. Campagne, and E. Devaux, "Electrical and mechanical properties of phenoxy/multiwalled carbon nanotubes multifilament yarn processed by melt spinning," *Text. Res. J.*, vol. 82, no. 20, pp. 2106–2115, 2012, doi: 10.1177/0040517512450760.
- [45] L. Marischal, A. Cayla, G. Lemort, C. Campagne, and É. Devaux, "Influence of melt spinning parameters on electrical conductivity of carbon fillers filled polyamide 12 composites," *Synth. Met.*, vol. 245, no. August, pp. 51–60, 2018, doi: 10.1016/j.synthmet.2018.08.003.
- [46] B. A. Alshammari, F. S. Al-Mubaddel, M. R. Karim, M. Hossain, A. S. Al-Mutairi, and A. N. Wilkinson, "Addition of graphite filler to enhance electrical, morphological, thermal, and mechanical properties in poly (ethylene terephthalate): Experimental characterization and material modeling," *Polymers (Basel)*, vol. 11, no. 9, pp. 1–20, 2019, doi: 10.3390/polym11091411.
- [47] J. Sanes, C. Sánchez, R. Pamies, M. D. Avilés, and M. D. Bermúdez, "Extrusion of polymer nanocomposites with graphene and graphene derivative nanofillers: An overview of recent developments," *Materials (Basel)*, vol. 13, no. 3, 2020, doi: 10.3390/ma13030549.
- [48] J. Militky, "The chemistry, manufacture and tensile behaviour of polyester fibers," *Handb. Tensile Prop. Text. Tech. Fibres*, pp. 223–314, 2009, doi: 10.1533/9781845696801.2.223.
- [49] R. R. Mather, *The structure of polyolefin fibres*, vol. 1. Woodhead Publishing Limited, 2009.
- [50] B. Zhu *et al.*, "Novel Polyethylene Fibers of Very High Thermal Conductivity Enabled by Amorphous Restructuring," *ACS Omega*, vol. 2, no. 7, pp. 3931–3944, 2017, doi: 10.1021/acsomega.7b00563.

- [51] A. Barot, A. A. Barot, T. M. Panchal, A. Patel, and C. M. Patel, "Polyester the Workhorse of Polymers: A Review from Synthesis to Recycling Chemical recycling of Textile Waste View project waterborn polyurethanes adhesive, coating and sealents View project Polyester the Workhorse of Polymers: A Review from Synthesis to ," no. October, 2019, [Online]. Available: www.scholarsresearchlibrary.com.
- [52] H. Radosch, *Poly(Butylene Terephthalate)*, no. Figure 1. 1970.
- [53] J. Y. Kim, "Poly(Butylene Terephthalate) Nanocomposites Containing Carbon Nanotube," *Mater. Sci.*, 2008.
- [54] E. Piesowicz, I. Irska, K. Bryll, K. Gawdzińska, and M. Bratychak, "Poly(butylene terephthalate/carbon nanotubes nanocomposites Part II. Structure and properties," *Polimery/Polymers*, vol. 61, no. 1, pp. 24–30, 2016, doi: 10.14314/polimery.2016.024.
- [55] C. Ślusarczyk, M. Sieradzka, J. Fabia, and R. Fryczkowski, "Supermolecular structure of poly(butylene terephthalate) fibers formed with the addition of reduced graphene oxide," *Polymers (Basel)*, vol. 12, no. 7, 2020, doi: 10.3390/polym12071456.
- [56] S. S. Hwang, "Tensile, electrical conductivity and EMI shielding properties of solid and foamed PBT/carbon fiber composites," *Compos. Part B Eng.*, vol. 98, pp. 1–8, 2016, doi: 10.1016/j.compositesb.2016.05.028.
- [57] S. Iijima, "Helical microtubes of graphitic carbon," *Nature*, vol. 368, pp. 444–446, 1994.
- [58] H. Golnabi, "Carbon nanotube research developments in terms of published papers and patents, synthesis and production," *Sci. Iran.*, vol. 19, no. 6, pp. 2012–2022, 2012, doi: 10.1016/j.scient.2012.10.036.
- [59] S. Rathinavel, K. Priyadarshini, and D. Panda, "A review on carbon nanotube: An overview of synthesis, properties, functionalization, characterization, and the application," *Mater. Sci. Eng. B Solid-State Mater. Adv. Technol.*, vol. 268, no. March, p. 115095, 2021, doi: 10.1016/j.mseb.2021.115095.
- [60] J. H. Du, J. Bai, and H. M. Cheng, "The present status and key problems of carbon nanotube based polymer composites," *Express Polym. Lett.*, vol. 1, no. 5, pp. 253–273, 2007, doi: 10.3144/expresspolymlett.2007.39.
- [61] Q. Cao, Q. Yu, D. W. Connell, and G. Yu, "Titania/carbon nanotube composite (TiO₂/CNT) and its application for removal of organic pollutants," *Clean Technol. Environ. Policy*, vol. 15, no. 6, pp. 871–880, 2013, doi: 10.1007/s10098-013-0581-y.
- [62] A. F. A. Trompeta, I. Preiss, F. Ben-Ami, Y. Benayahu, and C. A. Charitidis, "Toxicity

- testing of MWCNTs to aquatic organisms,” *RSC Adv.*, vol. 9, no. 63, pp. 36707–36716, 2019, doi: 10.1039/c9ra06672a.
- [63] Y. W. Yap *et al.*, “Recent Advances in Synthesis of Graphite from Agricultural Bio-Waste Material: A Review,” *Materials (Basel)*, vol. 16, no. 9, pp. 1–26, 2023, doi: 10.3390/ma16093601.
- [64] M. Warska, M. Barburski, and L. van Langenhove, “Textile elements for car seat to improve user’s driving comfort,” *J. Ind. Text.*, vol. 51, no. 4, pp. 513–539, 2021, doi: 10.1177/1528083719883061.
- [65] G. R. Kasaliwal, S. Pegel, A. Gödel, P. Pötschke Petra, and G. Heinrich, “Analysis of agglomerate dispersion mechanisms of multiwalled carbon nanotubes during melt mixing in polycarbonate,” *Polymer (Guildf)*, vol. 51, no. 12, pp. 2708–2720, 2010, doi: 10.1016/j.polymer.2010.02.048.
- [66] B. P. Saville, “Strength and elongation tests,” *Phys. Test. Text.*, pp. 115–167, 1999, doi: 10.1533/9781845690151.115.
- [67] H. Liu *et al.*, “Electrically conductive strain sensing polyurethane nanocomposites with synergistic carbon nanotubes and graphene bifillers,” *Nanoscale*, vol. 8, no. 26, pp. 12977–12989, 2016, doi: 10.1039/c6nr02216b.
- [68] J. Joseph, P. R. Munda, D. A. John, A. M. Sidpara, and J. Paul, “Graphene and CNT filled hybrid thermoplastic composites for enhanced EMI shielding effectiveness,” *Mater. Res. Express*, vol. 6, no. 8, 2019, doi: 10.1088/2053-1591/ab1e23.
- [69] A. Collet, A. Serghei, O. Lhost, Y. Trolez, P. Cassagnau, and R. Fulchiron, “Electrical conductivity under shear flow of molten polyethylene filled with carbon nanotubes: Experimental and modeling,” *Polym. Eng. Sci.*, vol. 61, no. 4, pp. 1129–1138, 2021, doi: 10.1002/pen.25651.

V. Appendix

1. Materials technical datasheet

1.1 PBT DuPont™ Crastin® FGS600F40 NC010

PRODUCT INFORMATION

DuPont™ Crastin® FGS600F40 NC010

THERMOPLASTIC POLYESTER RESIN

Product Information

Crastin® FGS600F40 NC010 is an unreinforced lubricated, low viscosity polybutylene terephthalate resin for injection moulding. It has been developed for consideration into applications such as parts for the food industry.

FOOD CONTACT

This product is manufactured according to Good Manufacturing Practice (GMP) principles and generally accepted in food contact applications in Europe and the USA when meeting applicable use conditions. For details, individual compliance statements are available from your DuPont representative.

General information	Value	Unit	Test Standard
Resin Identification	PBT	-	ISO 1043
Part Marking Code	>PBT<	-	ISO 11469
Rheological properties	Value	Unit	Test Standard
Melt mass-flow rate	33	g/10min	ISO 1133
Melt mass-flow rate, Temperature	250	°C	ISO 1133
Melt mass-flow rate, Load	2.16	kg	ISO 1133
Moulding shrinkage, parallel	1.6	%	ISO 294-4, 2577
Moulding shrinkage, normal	1.6	%	ISO 294-4, 2577
Mechanical properties	Value	Unit	Test Standard
Tensile Modulus	2400	MPa	ISO 527-1/-2
Yield stress	55	MPa	ISO 527-1/-2
Yield strain	4	%	ISO 527-1/-2
Nominal strain at break	30	%	ISO 527-1/-2
Strain at Break, 23°C, 50mm/min	>50	%	ISO 527-1/-2
Tensile creep modulus			ISO 899-1
1h	2600	MPa	
1000h	1800	MPa	
Charpy impact strength			ISO 179/1eU
23°C	N	kJ/m ²	
-30°C	N	kJ/m ²	
Charpy notched impact strength			ISO 179/1eA
23°C	4	kJ/m ²	
-30°C	4	kJ/m ²	
Thermal properties	Value	Unit	Test Standard
Melting temperature, 10°C/min	223	°C	ISO 11357-1/-3
Glass transition temperature, 10°C/min	55	°C	ISO 11357-1/-2
Temp. of deflection under load			ISO 75-1/-2
1.8 MPa	50	°C	
0.45 MPa	115	°C	
0.45 MPa, annealed	180	°C	
1.8 MPa, annealed	60	°C	
Vicat softening temperature, 50°C/h, 50N	175	°C	ISO 306
Coeff. of linear therm. expansion, parallel	110	E-6/K	ISO 11359-1/-2
Coeff. of linear therm. expansion, normal	120	E-6/K	ISO 11359-1/-2
Thermal conductivity of melt	0.21	W/(m K)	-
Spec. heat capacity of melt	2110	J/(kg K)	-
Flammability	Value	Unit	Test Standard
Burning Behav. at 1.5mm nom. thickn.	HB	class	IEC 60695-11-10
Thickness tested	1.5	mm	IEC 60695-11-10
Oxygen index	22	%	ISO 4589-1/-2
FMVSS Class	B	-	ISO 3795 (FMVSS 302)

DuPont™ Crastin® FGS600F40 NC010

THERMOPLASTIC POLYESTER RESIN

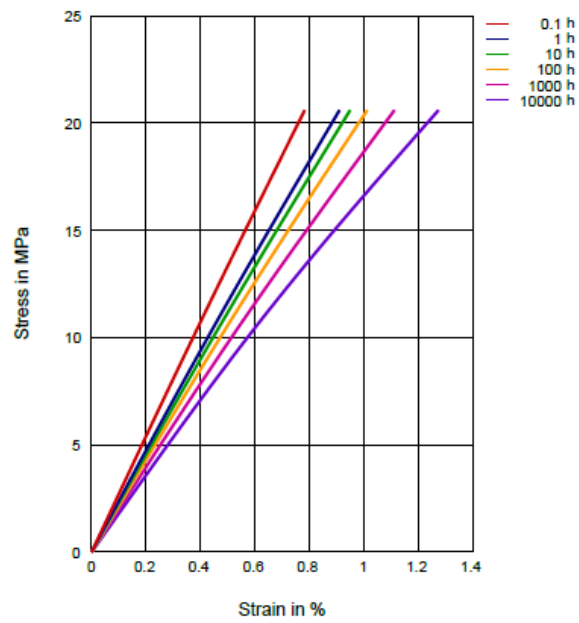
Burning rate, Thickness 1 mm	28	mm/min	ISO 3795 (FMVSS 302)
Electrical properties	Value	Unit	Test Standard
Relative permittivity, 1MHz	3.2	-	IEC 60250
Dissipation factor			IEC 60250
100Hz	20	E-4	
1MHz	200	E-4	
Volume resistivity	>1E13	Ohm*m	IEC 60093
Surface resistivity	1E12	Ohm	IEC 60093
Electric strength	26	kV/mm	IEC 60243-1
Comparative tracking index	600	-	IEC 60112
Other properties	Value	Unit	Test Standard
Humidity absorption, 2mm	0.2	%	Sim. to ISO 62
Water absorption, 2mm	0.4	%	Sim. to ISO 62
Density	1310	kg/m ³	ISO 1183
Density of melt	1110	kg/m ³	-
VDA Properties	Value	Unit	Test Standard
Odour	3	class	VDA 270
Fogging, F-value (refraction)	95	%	ISO 6452
Fogging, G-value (condensate)	0.2	mg	ISO 6452
Injection	Value	Unit	Test Standard
Drying Recommended	yes	-	-
Drying Temperature	120	°C	-
Drying Time, Dehumidified Dryer	2 - 4	h	-
Processing Moisture Content	≤0.04	%	-
Melt Temperature Optimum	250	°C	-
Min. melt temperature	240	°C	-
Max. melt temperature	260	°C	-
Mold Temperature Optimum	80	°C	-
Min. mould temperature	30	°C	-
Max. mould temperature	130	°C	-
Hold pressure range	≥60	MPa	-
Hold pressure time	4	s/mm	-
Back pressure	As low as possible		-
Ejection temperature	170	°C	-
Characteristics			
Processing	• Injection Moulding		
Delivery form	• Pellets		
Regional Availability	• North America	• Asia Pacific	• Near East/Africa
	• Europe	• South and Central America	• Global

DuPont™ Crastin® FGS600F40 NC010

THERMOPLASTIC POLYESTER RESIN

Diagrams

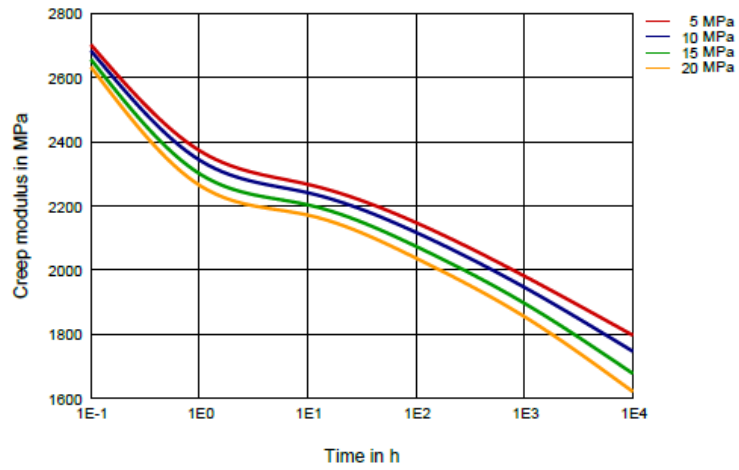
Stress-strain (isochronous) 23°C (measured on Crastin® S600F40 NC010)



DuPont™ Crastin® FGS600F40 NC010

THERMOPLASTIC POLYESTER RESIN

Creep modulus-time 23°C(measured on Crastin® S600F40 NC010)



DuPont™ Crastin® FGS600F40 NC010

THERMOPLASTIC POLYESTER RESIN

Chemical Media Resistance

Acids

- ✓ Acetic Acid (5% by mass) (23°C)
- ✓ Citric Acid solution (10% by mass) (23°C)
- ✓ Lactic Acid (10% by mass) (23°C)
- ✗ Hydrochloric Acid (36% by mass) (23°C)
- ✗ Nitric Acid (40% by mass) (23°C)
- ✗ Sulfuric Acid (38% by mass) (23°C)
- ✗ Sulfuric Acid (5% by mass) (23°C)
- ✗ Chromic Acid solution (40% by mass) (23°C)

Bases

- ✗ Sodium Hydroxide solution (35% by mass) (23°C)
- ✓ Sodium Hydroxide solution (1% by mass) (23°C)
- ✓ Ammonium Hydroxide solution (10% by mass) (23°C)

Alcohols

- ✓ Isopropyl alcohol (23°C)
- ✓ Methanol (23°C)
- ✓ Ethanol (23°C)

Hydrocarbons

- ✓ n-Hexane (23°C)
- ✓ Toluene (23°C)
- ✓ iso-Octane (23°C)

Ketones

- ✓ Acetone (23°C)

Ethers

- ✓ Diethyl ether (23°C)

Mineral oils

- ✓ SAE 10W40 multigrade motor oil (23°C)
- ✗ SAE 10W40 multigrade motor oil (130°C)
- ✗ SAE 80/90 hypoid-gear oil (130°C)
- ✓ Insulating Oil (23°C)

Standard Fuels

- ✗ ISO 1817 Liquid 1 - E5 (60°C)
- ✗ ISO 1817 Liquid 2 - M15E4 (60°C)
- ✗ ISO 1817 Liquid 3 - M3E7 (60°C)
- ✗ ISO 1817 Liquid 4 - M15 (60°C)
- ✓ Standard fuel without alcohol (pref. ISO 1817 Liquid C) (23°C)
- ✓ Standard fuel with alcohol (pref. ISO 1817 Liquid 4) (23°C)

DuPont™ Crastin® FGS600F40 NC010

THERMOPLASTIC POLYESTER RESIN

- ✓ Diesel fuel (pref. ISO 1817 Liquid F) (23°C)
- ✓ Diesel fuel (pref. ISO 1817 Liquid F) (90°C)
- ✗ Diesel fuel (pref. ISO 1817 Liquid F) (>90°C)

Salt solutions

- ✓ Sodium Chloride solution (10% by mass) (23°C)
- ✓ Sodium Hypochlorite solution (10% by mass) (23°C)
- ✓ Sodium Carbonate solution (20% by mass) (23°C)
- ✓ Sodium Carbonate solution (2% by mass) (23°C)
- ✓ Zinc Chloride solution (50% by mass) (23°C)

Other

- ✓ Ethyl Acetate (23°C)
- ✗ Hydrogen peroxide (23°C)
- ✗ DOT No. 4 Brake fluid (130°C)
- ✗ Ethylene Glycol (50% by mass) in water (108°C)
- ✓ 1% nonylphenoxy-polyethyleneoxy ethanol in water (23°C)
- ✓ 50% Oleic acid + 50% Olive Oil (23°C)
- ✓ Water (23°C)
- ✗ Water (90°C)
- ✓ Phenol solution (5% by mass) (23°C)

Symbols used:

- ✓ possibly resistant

Defined as: Supplier has sufficient indication that contact with chemical can be potentially accepted under the intended use conditions and expected service life. Criteria for assessment have to be indicated (e.g. surface aspect, volume change, property change).

- ✗ not recommended - see explanation

Defined as: Not recommended for general use. However, short-term exposure under certain restricted conditions could be acceptable (e.g. fast cleaning with thorough rinsing, spills, wiping, vapor exposure).

Contact DuPont for Material Safety Data Sheet, general guides and/or additional information about ventilation, handling, purging, drying, etc. ISO Mechanical properties measured at 4mm (Hytrel® measured at 2 mm), IEC Electrical properties measured at 2mm, all ASTM properties measured at 3.2mm, and test temperatures are 23°C unless otherwise stated.

The information set forth herein is furnished free of charge and is based on technical data that DuPont believes to be reliable and falls within the normal range of properties. It is intended for use by persons having technical skill, at their own discretion and risk. This data should not be used to establish specification limits nor used alone as the basis of design. Handling precaution information is given with the understanding that those using it will satisfy themselves that their particular conditions of use present no health or safety hazards. Since conditions of product use and disposal are outside our control, we make no warranties, express or implied, and assume no liability in connection with any use of this information. As with any product, evaluation under end-use conditions prior to specification is essential. Nothing herein is to be taken as a license to operate or a recommendation to infringe on patents. Caution: Do not use in medical applications involving permanent implantation in the human body. For other medical applications, discuss with your DuPont customer representative and read Medical Caution H-50103-4.

Copyright © 2015 DuPont or its affiliates. All Rights Reserved. The DuPont Oval Logo, DuPont™, The miracles of science™ and all products denoted with © or ™ are registered trademarks or trademarks of E.I. du Pont de Nemours and Company or its affiliates.

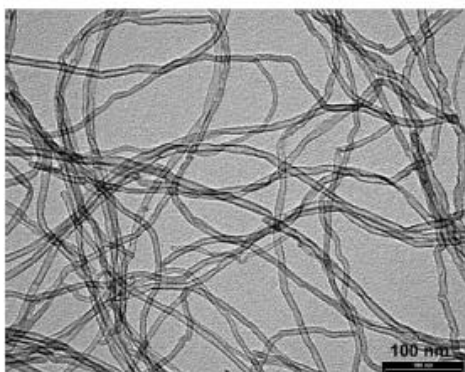
1.2 NANOCYL® NC7000™ MWCNTs technical datasheet



Ref: NANOCYL™ NC7000 – 10 March 2009 - V05

NANOCYL™ NC7000 series - Product Datasheet – Thin Multi-Wall Carbon Nanotubes

General information



NANOCYL™ NC7000 series, thin multi-wall carbon nanotubes, are produced via the catalytic carbon vapor deposition (CCVD) process.

A primary interest is in applications requiring low electrical percolation threshold such as high-performance electrostatic dissipative plastics or coatings.

NC7000 is available in powder form in quantities starting at 2 kg to multi-tons.

Pre-dispersed forms are also available (PLASTICYL™, EPOCYL™, AQUACYL™).

Characterization NC7000

PROPERTY	UNIT	VALUE	METHOD OF MEASUREMENT
Average Diameter	nanometers	9.5	TEM
Average Length	microns	1.5	TEM
Carbon Purity	%	90	TGA
Metal Oxide	%	10	TGA
Amorphous Carbon	-	*	HRTEM
Surface Area	m ² /g	250-300	BET

* Pyrolytically deposited carbon on the surface of the NC7000

+ Further information is available upon request

The information contained on this datasheet is believed to be reliable—yet Nanocyl makes no warranties and assumes no liability in connection with any use of this information. Nothing herein is to be taken as a license to operate under or infringe any patent. While this information is accurate at the time of publication, please contact Nanocyl or check <http://www.nanocyl.com> for the most up-to-date information.

Nanocyl S.A.

Rue de l'Essor 4
B-5060 Sambreville
BELGIUM

Tel. +32 71 750 380

Fax +32 71 750 390

sales@nanocyl.com

US contact

info-us@nanocyl.com

www.nanocyl.com

1.3 Graphite GraphTHERM® 23/99.9 technical datasheet



Schöne Aussicht 39
65396 Walluf

TECHNICAL DATA SHEET

Telefon: +49 (0) 6123 798-0
Telefax: +49 (0) 6123 798-44
E-Mail: office@luh.de
Internet: www.luh.de

GraphTHERM® 23/99.9

C-Content:	min.	99,9 %
Ash:	max.	0,1 %
Moisture:	max.	0,5 %
Fe:	max.	100 ppm
Tamped Density:		0,95 – 1,05 g/cm ³
BET Surface Area:		5 – 6,5 m ² /g
Particle Size:	D ₁₀	10 – 14 µm
	D ₅₀	21 – 25 µm
	D ₉₀	40 – 50 µm

1.4 CI 1036 Highly Conductive Silver Ink technical datasheet



Engineered Conductive Materials, LLC
An Engineered Materials Systems, Inc. Company

132 Johnson Drive
Delaware, Ohio 43015-8699
Tel: (740) 362-4444
Fax: (740) 362-4433
www.conductives.com

Technical Data Sheet

CI-1036

**Highly Conductive, Highly
Flexible Silver Ink**

DESCRIPTION	CI-1036 is silver conductive ink designed for superior durability and crease resistance along with low resistance and long screen residence time. The main uses of CI-1036 are for switches that are subject to deformation e.g. poly-doming or intentional creasing or flexing e.g. tail fold-over. CI-1036 shows excellent adhesion to print treated polyester.	
ADVANTAGES	<ul style="list-style-type: none">✓ Excellent abrasion resistance✓ Extended screen residence	<ul style="list-style-type: none">✓ Extremely flexible✓ Highly conductive
TYPICAL UNCURED PROPERTIES	Color Viscosity Total Solids Content Density Flash Point VOC	Silver 10,000 CPS 25°C #51 20 rpm 66% 17.3 lbs/gallon (2.08 kg/l) 230°F (110°C) Tag Closed Cup 703.8 grams of solvent/liter
TYPICAL CURED PROPERTIES	Electrical Resistance Theoretical Coverage	< 0.010 ohms/square @ 1.0 mil < 0.010 ohms/square @ 25.4 microns Cured 10 Minutes at 248 F (120 C) 485.2 ft ² /Gal/Mil 5.74 m ² /kilogram/25.4 microns

**APPLICATION
INFORMATION**

- Target 0.0003” (8µm) dry film thickness (range 7-15 µm per application requirements).
- Screen recommendations:
 - Polyester mesh 156 – 206 threads/in (61-81T/cm)
 - Stainless mesh 173 – 330 threads/in (68-130T/cm)
 - Emulsion 0.0004 – 0.0016” (10-40 µm)
 - Solvent resistant, ≥5µm EOM, direct or capillary
 - Screen tension ≥ 25 N/cm
- Current screen trends offer higher mesh counts with greater % open, high tension and emulsion options to deliver finer lines at thicker deposits.
- Squeegee: solvent resistant, high durometer (70-80), sharp edge.
- Ink preconditioning: gently hand stir with a spatula for 1-2 minutes, and ensure that the ink has reached room temperature. This conditions the viscosity to that seen during screen action. DO NOT use a high velocity / high shear mixer which can induce air bubbles or damage rheology.

**CURE
SCHEDULE**

CI-1036 does not require any leveling time and can be forced cured immediately after printing. Typical forced curing is for 10 minutes at 248°F (120°C). Various time temperature combinations can be used.

Complete cure can be confirmed by re-curing the print a second time and testing the electrical resistance. The electrical resistance should not decrease by more than 10%. If the resistance does decrease more than 10%, increase oven temperature or decrease belt speed.

CLEAN UP

CI-1036 can be cleaned up with M.E.K (Methyl Ethyl Ketone) or a blend of solvents that will completely clean a cured film. Screens and printing tools should be allowed to dry completely before reuse.

**STORAGE AND
HANDLING**

- Shelf life is six (6) months, unopened container, stored < 55°F (15°C).
- Store product < 55°F (15°C) for maximum shelf life and minimal solvent loss. Avoid high temperature exposure.

**HEALTH AND
SAFETY**

- Use with adequate ventilation.
- Avoid skin contact.
- If ingested, consult a physician immediately.
- Consult the product Material Safety Data Sheet for additional information.

**APPLICATION
ASSISTANCE**

ECM’s application specialists are available to assist you in production start-up with CI-1036. For more information, please call ECM at 1.740.362.4444.

2. Characterization data

2.1 Melt flow index data

Neat PBT				
Test	MFR (g/10 min)	MVR (cm³/10 min)	Melt density (g/cm³)	Mass (g)
1	53,334	48,306	1,104	2,354
2	54,669	51,243	1,067	2,270
3	51,916	47,162	1,101	2,347
4	55,086	50,191	1,098	2,340
5	55,625	52,614	1,057	2,254
Average	54,126	49,903	1,085	2,313
SD	1,340	1,964	0,019	0,042

PBT/3%CNTs				
Test	MFR (g/10 min)	MVR (cm³/10 min)	Melt density (g/cm³)	Mass (g)
1	11,741	10,625	1,105	2,356
2	12,272	11,077	1,108	2,362
3	11,599	10,715	1,083	2,308
4	13,205	11,860	1,113	2,374
5	14,843	13,811	1,075	2,290
6	13,634	12,301	1,108	2,363
7	13,943	12,591	1,107	2,361
Average	13,034	11,854	1,106	2,345
SD	0,266	0,226	0,001	0,003

Reprocessed PBT/3%CNTs				
Test	MFR (g/10 min)	MVR (cm³/10 min)	Melt density (g/cm³)	Mass (g)
1	13,433	12,110	1,109	2,365
2	14,138	13,016	1,086	2,316
3	16,252	15,211	1,068	2,278
4	14,333	12,921	1,109	2,365
5	14,303	12,921	1,107	2,360
6	15,546	14,299	1,087	2,318
7	15,821	14,421	1,097	2,339
Average	14,832	13,557	1,093	2,334
SD	0,899	0,951	0,013	0,028

2.2 Mechanical tests data

OS_01			
Name	Maximum Force	Elongation at break	Tenacity
Unit	cN	%	cN/dtex
R1	997	256	1,13
R2	1062	281	1,20
R3	1105	270	1,25
R4	1065	264	1,20
R5	1057	250	1,19
R6	927	231	1,05
R7	971	235	1,10
R8	1026	291	1,16
R9			FALSE
R10			FALSE
dtex	885		

OS_02			
Name	Maximum Force	Elongation at break	Tenacity
Unit	cN	%	cN/dtex
R1	915,322	7,45303	0,42
R2	900,633	10,3043	0,42
R3	795,494	9,2258	0,37
R4	890,15	10,3601	0,41
R5	937,994	7,34307	0,43
R6	963	11	0,44
R7	963	10	0,44
R8	898,81	9,91483	0,41
R9			FALSE
R10			FALSE
dtex	2168		

OS_03			
Name	Maximum Force	Elongation at break	Tenacity
Unit	cN	%	cN/dtex
R1	1199,35	10,3036	0,48
R2	1260,41	10,093	0,51
R3	1186,86	8,91237	0,48
R4	1184,03	10,3617	0,48
R5	1272	10	0,51
R6	1161	10	0,47
R7	1274	9	0,51
R8	1262	10	0,51
R9	1182	8	0,48
R10			FALSE
dtex	2487		

OS_04			
Name	Maximum Force	Elongation at break	Tenacity
Unit	cN	%	cN/dtex
R1	1526,6	9,64893	0,49
R2	1553,86	9,13473	0,50
R3	1503,67	9,5532	0,48
R4	1501	9	0,48
R5	1477	9	0,47
R6	1468	11	0,47
R7	1468	8	0,47
R8	1406,21	9,29873	0,45
R9			FALSE
R10			FALSE
dtex	3135		

OS_05			
Name	Maximum Force	Elongation at break	Tenacity
Unit	cN	%	cN/dtex
R1	945,61	8,0503	0,57
R2	945,153	9,6009	0,57
R3	986,293	10,2851	0,59
R4	969	8	0,58
R5	916	9	0,55
R6	929,018	9,15907	0,56
R7	948,878	8,81017	0,57
R8	933,333	8,92997	0,56
R9	970,843	10,8646	0,58
R10			FALSE
dtex	1667		

OS_06			
Name	Maximum Force	Elongation at break	Tenacity
Unit	cN	%	cN/dtex
R1	1223,75	11,3358	0,40
R2	1165,55	9,6707	0,38
R3	1279	10	0,41
R4	1356,82	10,2795	0,44
R5	1194,46	10,9608	0,39
R6	1353,13	10,166	0,44
R7	1205,08	10,1304	0,39
R8	1227,95	9,29847	0,40
R9	1263,21	10,883	0,41
R10			FALSE
dtex	3090		

OS_07			
Name	Maximum Force	Elongation at break	Tenacity
Unit	cN	%	cN/dtex
R1	1514	10	0,54
R2	1434,97	7,895	0,51
R3	1541,95	9,61263	0,55
R4	1411,69	8,4471	0,50
R5	1390,35	7,93217	0,49
R6	1583,95	8,23287	0,56
R7	1336,29	9,43367	0,47
R8	1453,64	8,76803	0,51
R9	1635,7	9,28587	0,58
R10			FALSE
dtex	2829		

	Tenacity (cN/dtex)			Elongation at break (%)			Maximum Force (cN)		
	AV	SD	CV	AV	SD	CV	AV	SD	CV
OS_01	1,16	0,06	0,05	259,6	20	0,08	1026	55	0,05
OS_02	0,42	0,02	0,06	9,4	1	0,13	908	50	0,06
OS_03	0,49	0,02	0,04	9,6	1	0,07	1220	43	0,04
OS_04	0,47	0,01	0,03	9,2	1	0,07	1488	42	0,03
OS_05	0,57	0,01	0,02	9,2	1	0,10	949	21	0,02
OS_06	0,41	0,02	0,05	10,3	1	0,06	1252	64	0,05
OS_07	0,52	0,03	0,06	8,9	1	0,08	1478	92	0,06

2.3 Electrical characterization data

PBT/CNTs

		mm			Resistance (Ohm)	Resistivity (Ohm.m)	Conductivity (S/m)	AV	SD	CV (%)
		d ₁	d ₂	AV						
PBT/5%CNTs	1	2,15	2,17	2,16	1,46574E-05	5,88E+02	5,74E-01	1,75E+00	0,270	15,371
	2	2,2	2,17	2,185	1,49987E-05	7,20E+02	7,20E-01			
	3	2,18	2,15	2,165	1,47254E-05	6,62E+02	6,50E-01			
	4	2,11	2,14	2,125	1,41863E-05	6,05E+02	5,72E-01			
	5	2,13	2,19	2,16	1,46574E-05	5,43E+02	5,31E-01			
	6	2,17	2,15	2,16	1,46574E-05	6,19E+02	6,05E-01			
	7	2,11	2,15	2,13	1,42531E-05	6,35E+02	6,03E-01			
	8	2,21	2,18	2,195	1,51363E-05	4,55E+02	4,59E-01			
	9	2,15	2,18	2,165	1,47254E-05	4,51E+02	4,43E-01			
	10	2,22	2,19	2,205	1,52745E-05	6,62E+02	6,74E-01			
PBT/4%CNTs	1	2,22	2,2	2,21	1,53439E-05	6,84E+02	7,00E-01	1,03E+00	0,228	22,016
	2	2,19	2,25	2,22	1,5483E-05	1,07E+03	1,11E+00			
	3	2,18	2,2	2,19	1,50674E-05	9,75E+02	9,79E-01			
	4	2,23	2,26	2,245	1,58337E-05	8,81E+02	9,30E-01			
	5	2,17	2,19	2,18	1,49301E-05	8,10E+02	8,06E-01			
	6	2,26	2,26	2,26	1,6046E-05	9,14E+02	9,78E-01			
	7	2,25	2,27	2,26	1,6046E-05	7,46E+02	7,98E-01			
	8	2,2	2,23	2,215	1,54134E-05	1,69E+03	1,74E+00			
	9	2,19	2,2	2,195	1,51363E-05	1,19E+03	1,20E+00			
	10	2,21	2,24	2,225	1,55528E-05	9,70E+02	1,01E+00			

		mm			Area (m ²)	Resistance (Ohm)	Resistivity (Ohm.m)	Conductivity (S/m)	AV	SD	CV (%)
		d ₁	d ₂	AV							
PBT/3,5%CNTs	1	2,11	2,15	2,13	1,42531E-05	1,94E+03	1,84E+00	5,44E-01	5,26E-01	0,113	21,541
	2	2,17	2,12	2,145	1,44545E-05	1,90E+03	1,83E+00	5,46E-01			
	3	2,21	2,2	2,205	1,52745E-05	1,58E+03	1,61E+00	6,22E-01			
	4	2,17	2,17	2,17	1,47934E-05	2,52E+03	2,48E+00	4,03E-01			
	5	2,2	2,25	2,225	1,55528E-05	2,21E+03	2,29E+00	4,36E-01			
	6	2,14	2,18	2,16	1,46574E-05	1,73E+03	1,69E+00	5,93E-01			
	7	2,22	2,21	2,215	1,54134E-05	2,01E+03	2,07E+00	4,83E-01			
	8	2,15	2,17	2,16	1,46574E-05	1,40E+03	1,37E+00	7,31E-01			
	9	2,18	2,15	2,165	1,47254E-05	1,73E+03	1,70E+00	5,88E-01			
	10	2,18	2,18	2,18	1,49301E-05	3,16E+03	3,15E+00	3,18E-01			
PBT/3%CNTs	1	2,18	2,2	2,19	1,50674E-05	7,51E+03	7,54E+00	1,33E-01	2,87E-01	0,074	25,865
	2	2,19	2,2	2,195	1,51363E-05	2,62E+03	2,64E+00	3,79E-01			
	3	2,16	2,23	2,195	1,51363E-05	2,42E+03	2,44E+00	4,10E-01			
	4	2,19	2,19	2,19	1,50674E-05	4,02E+03	4,04E+00	2,48E-01			
	5	2,2	2,19	2,195	1,51363E-05	4,12E+03	4,16E+00	2,41E-01			
	6	2,1	2,19	2,145	1,44545E-05	3,54E+03	3,41E+00	2,94E-01			
	7	2,1	2,17	2,135	1,43201E-05	3,97E+03	3,79E+00	2,64E-01			
	8	2,17	2,17	2,17	1,47934E-05	3,16E+03	3,12E+00	3,21E-01			
	9	2,23	2,14	2,185	1,49987E-05	3,07E+03	3,07E+00	3,26E-01			
	10	2,16	2,15	2,155	1,45896E-05	3,97E+03	3,87E+00	2,59E-01			

		mm			Area (m ²)	Resistance (Ohm)	Resistivity (Ohm.m)	Conductivity (S/m)	AV	SD	CV (%)
		d ₁	d ₂	AV							
PBT/2%CNTs	1	2,2	2,2	2,2	1,52053E-05	9,17E+04	9,30E+01	1,08E-02	2,61E-02	0,0128	49,144
	2	2,2	2,2	2,2	1,52053E-05	1,04E+05	1,06E+02	9,46E-03			
	3	2,14	2,16	2,15	1,4522E-05	3,13E+04	3,03E+01	3,31E-02			
	4	2,14	2,15	2,145	1,44545E-05	4,37E+04	4,21E+01	2,37E-02			
	5	2,15	2,15	2,15	1,4522E-05	3,11E+04	3,01E+01	3,32E-02			
	6	2,17	2,18	2,175	1,48617E-05	2,85E+04	2,82E+01	3,55E-02			
	7	2,2	2,2	2,2	1,52053E-05	3,38E+04	3,43E+01	2,92E-02			
	8	2,18	2,17	2,175	1,48617E-05	3,86E+04	3,82E+01	2,61E-02			
	9	2,2	2,19	2,195	1,51363E-05	1,93E+04	1,94E+01	5,14E-02			
	10	2,14	2,14	2,14	1,43872E-05	1,17E+05	1,12E+02	8,93E-03			
PBT/1%CNTs	1	2,21	2,2	2,205	1,52745E-05	3,50E+09	3,56E+06	2,81E-07	1,91E-05	4,34E-05	227,972
	2	2,17	2,18	2,175	1,48617E-05	1,70E+09	1,68E+06	5,94E-07			
	3	2,2	2,19	2,195	1,51363E-05	1,60E+09	1,61E+06	6,19E-07			
	4	2,19	2,17	2,18	1,49301E-05	2,53E+09	2,52E+06	3,97E-07			
	5	2,15	2,17	2,16	1,46574E-05	5,00E+08	4,89E+05	2,05E-06			
	6	2,2	2,17	2,185	1,49987E-05	2,30E+09	2,30E+06	4,35E-07			
	7	2,21	2,17	2,19	1,50674E-05	4,90E+08	4,92E+05	2,03E-06			
	8	2,16	2,16	2,16	1,46574E-05	3,88E+07	3,79E+04	2,64E-05			
	9	2,2	2,21	2,205	1,52745E-05	6,67E+06	6,79E+03	1,47E-04			
	10	2,16	2,17	2,165	1,47254E-05	9,70E+07	9,52E+04	1,05E-05			

PBT/CNTs/G

		mm			Area (m ²)	Resistance (Ohm)	Resistivity (Ohm.m)	Conductivity (S/m)	AV	SD	CV (%)
		d ₁	d ₂	AV							
PBT/2%CNTs/1%G	1	2,08	2,02	2,05	1,32025E-05	5,75E+07	5,06E+04	1,98E-05	2,67E-05	1,25E-05	46,900
	2	2,07	2,06	2,065	1,33965E-05	5,28E+07	4,72E+04	2,12E-05			
	3	2,06	2,1	2,08	1,35918E-05	4,05E+07	3,67E+04	2,72E-05			
	4	2,09	2,06	2,075	1,35265E-05	5,10E+07	4,60E+04	2,17E-05			
	5	2,07	2,05	2,06	1,33317E-05	5,50E+07	4,89E+04	2,05E-05			
	6	1,98	2,06	2,02	1,2819E-05	4,38E+07	3,74E+04	2,67E-05			
	7	1,98	2,06	2,02	1,2819E-05	3,23E+07	2,76E+04	3,62E-05			
	8	2,07	2	2,035	1,301E-05	9,66E+07	8,38E+04	1,19E-05			
	9	2,07	2	2,035	1,301E-05	1,93E+07	1,67E+04	5,97E-05			
	10	2,03	2	2,015	1,27556E-05	5,39E+07	4,58E+04	2,18E-05			
PBT/2%CNTs/2%G	1	2,07	2,1	2,085	1,36572E-05	2,30E+06	2,09E+03	4,78E-04	2,49E-04	0,0002	78,931
	2	2,1	2,14	2,12	1,41196E-05	1,80E+06	1,69E+03	5,90E-04			
	3	2,1	2,08	2,09	1,37228E-05	2,90E+06	2,65E+03	3,77E-04			
	4	2,13	2,12	2,125	1,41863E-05	2,60E+06	2,46E+03	4,07E-04			
	5	2,05	2,08	2,065	1,33965E-05	1,95E+08	1,74E+05	5,74E-06			
	6	2,11	2,04	2,075	1,35265E-05	1,80E+07	1,62E+04	6,16E-05			
	7	2,08	2,11	2,095	1,37885E-05	1,10E+07	1,01E+04	9,89E-05			
	8	2,04	2,03	2,035	1,301E-05	4,30E+07	3,73E+04	2,68E-05			
	9	2,09	2,08	2,085	1,36572E-05	3,90E+06	3,55E+03	2,82E-04			
	10	2,06	2,04	2,05	1,32025E-05	7,10E+06	6,25E+03	1,60E-04			

		mm			Resistance (Ohm)	Resistivity (Ohm.m)	Conductivity (S/m)	AV	SD	CV (%)	
		d ₁	d ₂	AV							Area (m ²)
PBT/2%CNTs/5%G	1	1,94	1,91	1,925	1,16416E-05	2,25E+07	1,75E+04	5,73E-05	3,97E-04	0,0004	105,503
	2	1,95	1,9	1,925	1,16416E-05	3,19E+07	2,47E+04	4,04E-05			
	3	1,96	1,92	1,94	1,18237E-05	4,33E+07	3,41E+04	2,93E-05			
	4	1,92	1,94	1,93	1,17021E-05	1,37E+06	1,07E+03	9,36E-04			
	5	1,89	1,94	1,915	1,15209E-05	5,02E+06	3,86E+03	2,59E-04			
	6	1,94	1,88	1,91	1,14608E-05	4,00E+06	3,06E+03	3,27E-04			
	7	1,88	1,94	1,91	1,14608E-05	3,90E+06	2,98E+03	3,36E-04			
	8	1,88	1,94	1,91	1,14608E-05	5,20E+07	3,97E+04	2,52E-05			
	9	1,88	1,92	1,9	1,13411E-05	2,10E+06	1,59E+03	6,30E-04			
	10	1,91	1,95	1,93	1,17021E-05	9,67E+05	7,54E+02	1,33E-03			

Reprocessed PBT/CNTs/G

		mm			Resistance (Ohm)	Resistivity (Ohm.m)	Conductivity (S/m)	AV	SD	CV (%)	
		d ₁	d ₂	AV							Area (m ²)
PBT/2%CNTs/1%G	1	2,2	2,29	2,245	1,58337E-05	3,12E+07	3,29E+04	3,04E-05	1,30E-05	8,55E-06	6,75E+01
	2	2,28	2,31	2,295	1,65468E-05	2,61E+08	2,87E+05	3,48E-06			
	3	2,2	2,24	2,22	1,5483E-05	4,33E+07	4,47E+04	2,24E-05			
	4	2,28	2,26	2,27	1,61883E-05	6,90E+07	7,45E+04	1,34E-05			
	5	2,19	2,24	2,215	1,54134E-05	7,07E+07	7,26E+04	1,38E-05			
	6	2,25	2,27	2,26	1,6046E-05	5,30E+10	5,67E+07	1,76E-08			
	7	2,26	2,26	2,26	1,6046E-05	1,99E+08	2,13E+05	4,70E-06			
	8	2,29	2,22	2,255	1,59751E-05	5,74E+07	6,11E+04	1,64E-05			
	9	2,25	2,25	2,25	1,59043E-05	7,80E+07	8,27E+04	1,21E-05			
	10	2,23	2,18	2,205	1,52745E-05	7,26E+07	7,39E+04	1,35E-05			

		mm			Resistance (Ohm)	Resistivity (Ohm.m)	Conductivity (S/m)	AV	SD	CV (%)
		d ₁	d ₂	AV						
PBT/2%CNTs/2%G	1	2,28	2,24	2,26	1,6046E-05	7,35E+07	7,86E+04	3,00E-06	3,40E-06	1,14E+02
	2	2,29	2,19	2,24	1,57633E-05	1,30E+09	1,37E+06			
	3	2,19	2,24	2,215	1,54134E-05	3,30E+09	3,39E+06			
	4	2,22	2,2	2,21	1,53439E-05	3,67E+09	3,75E+06			
	5	2,21	2,31	2,26	1,6046E-05	4,10E+08	4,39E+05			
	6	2,28	2,34	2,31	1,67639E-05	3,43E+08	3,83E+05			
	7	2,25	2,29	2,27	1,61883E-05	4,20E+08	4,53E+05			
	8	2,21	2,23	2,22	1,5483E-05	2,98E+08	3,08E+05			
	9	2,22	2,26	2,24	1,57633E-05	3,50E+08	3,68E+05			
	10	2,25	2,2	2,225	1,55528E-05	3,34E+08	3,46E+05			
PBT/2%CNTs/5%G	1	2,11	2,19	2,15	1,4522E-05	1,42E+08	1,37E+05	2,03E-05	3,01E-05	1,49E+02
	2	2,16	2,13	2,145	1,44545E-05	3,22E+07	3,10E+04			
	3	2,17	2,13	2,15	1,4522E-05	2,12E+08	2,05E+05			
	4	2,19	2,13	2,16	1,46574E-05	5,00E+07	4,89E+04			
	5	2,15	2,14	2,145	1,44545E-05	5,24E+07	5,04E+04			
	6	2,22	2,25	2,235	1,5693E-05	2,20E+08	2,30E+05			
	7	2,2	2,16	2,18	1,49301E-05	2,99E+08	2,98E+05			
	8	2,18	2,18	2,18	1,49301E-05	9,50E+06	9,46E+03			
	9	2,18	2,21	2,195	1,51363E-05	2,23E+08	2,25E+05			
	10	2,18	2,18	2,18	0,149301049	1,50E+09	1,49E+10			

PBT/3%CNTs multifilament fibers

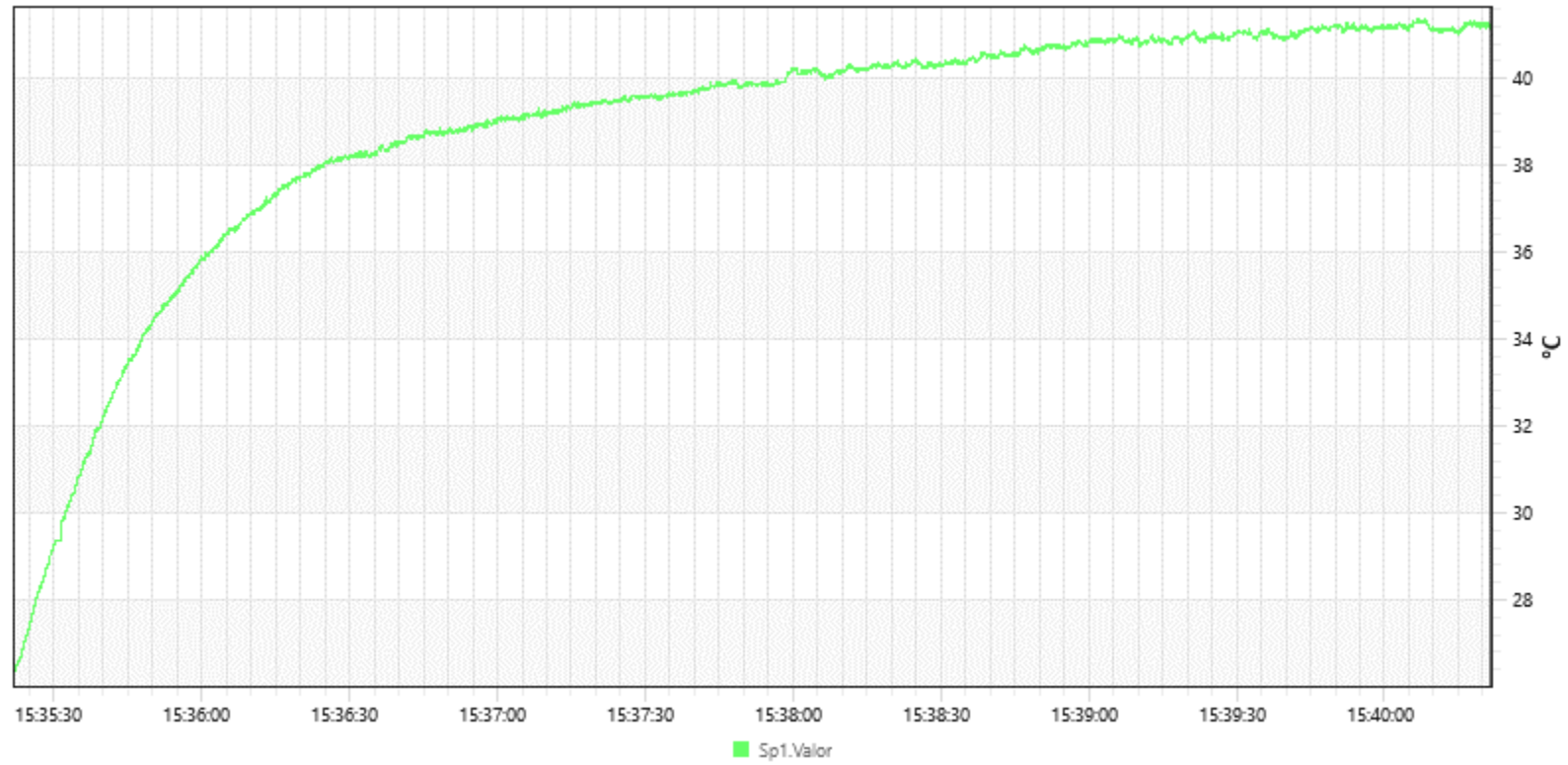
Bobbin	OS_02	OS_03	OS_04	OS_05	OS_06	OS_07
Diameter (µm)	700,8	817,3	805,6	655,6	676,2	926,2
	686,4	796,8	826,2	648,1	707	929,6
	691,9	821,4	829,6	648,1	739,2	922,1
	737,1	833,7	806,3	649,5	759,7	918
	877,6	711,8	757,7	661,8	953,6	953,6
	855,1	727,5	741,9	661,8	894	949,5
	809,1	760,4	741,9	661,8	890,6	953,6
	837,9	776,9	757,7	656,3	874,9	961,1
	913,9	756,3	794	914,5	866,6	1000,9
	961,1	744	773,4	914,5	862,5	961,1
	935,8	763,8	749,4	910,4	866,6	976,9
	964,6	764,6	749,5	898,1	870,7	823,4
	642,6	767,9	746	799,5	870,7	827,5
	619,3	800,8	713,8	798,8	866,7	827,5
	618,6	800,9	705,6	806,3	874,2	839,2
	650,8	820,7	697,4	787,1	835,1	874,8
	792,6	822,1	970	767,3	783,7	898,1
	716	789,9	874,1	759,1	768,7	913,9
	675,5	781,6	854,3	751,5	776,2	910,5
	671,3	765,9	818	794,7	791,9	898,8
Average diameter (m)	0,0007679	0,000781215	0,00078562	0,00075724	0,00082644	0,000913315

Bobbin	Conditions	Diameter (m)	Area (m²)	Resistance (Ohm)	Resistivity (Ohm.m)	Conductivity (S/m)	AV	SD	CV
OS_2	Bomba: 10 rpm Rolo 1: 100 m/min Rolo 2: 100 m/min Rolo 3: 100 m/min CDR: 1 DDR: 35	0,00077	0,00000046	3,60E+08	5,56E+03	1,80E-04	1,40E-04	1,24E-04	0,885
				1,75E+09	2,70E+04	3,70E-05			
				7,00E+08	1,08E+04	9,25E-05			
				1,78E+08	2,75E+03	3,64E-04			
				2,30E+09	3,55E+04	2,82E-05			
OS_3	Bomba: 14 rpm Rolo 1: 100 m/min Rolo 2: 100 m/min Rolo 3: 100 m/min CDR: 1 DDR: 25	0,00078	0,00000048	1,00E+09	1,60E+04	6,26E-05	3,49E-05	1,50E-05	0,428
				2,90E+09	4,63E+04	2,16E-05			
				2,80E+09	4,47E+04	2,24E-05			
				2,00E+09	3,20E+04	3,13E-05			
				1,70E+09	2,72E+04	3,68E-05			
OS_4	Bomba: 18 rpm Rolo 1: 100 m/min Rolo 2: 100 m/min Rolo 3: 100 m/min CDR: 1 DDR: 20	0,00079	0,00000048	2,05E+09	3,31E+04	3,02E-05	1,75E-05	6,83E-06	0,390
				5,00E+09	8,08E+04	1,24E-05			
				3,80E+09	6,14E+04	1,63E-05			
				5,70E+09	9,21E+04	1,09E-05			
				3,50E+09	5,66E+04	1,77E-05			
OS_5	Bomba: 10 rpm Rolo 1: 100 m/min Rolo 2: 100 m/min Rolo 3: 100 m/min CDR: 1 DDR: 35	0,00076	0,00000045	2,33E+08	3,50E+03	2,86E-04	2,86E-04	5,01E-05	0,175
				2,50E+08	3,75E+03	2,66E-04			
				3,20E+08	4,80E+03	2,08E-04			
				1,85E+08	2,78E+03	3,60E-04			
				2,14E+08	3,21E+03	3,11E-04			

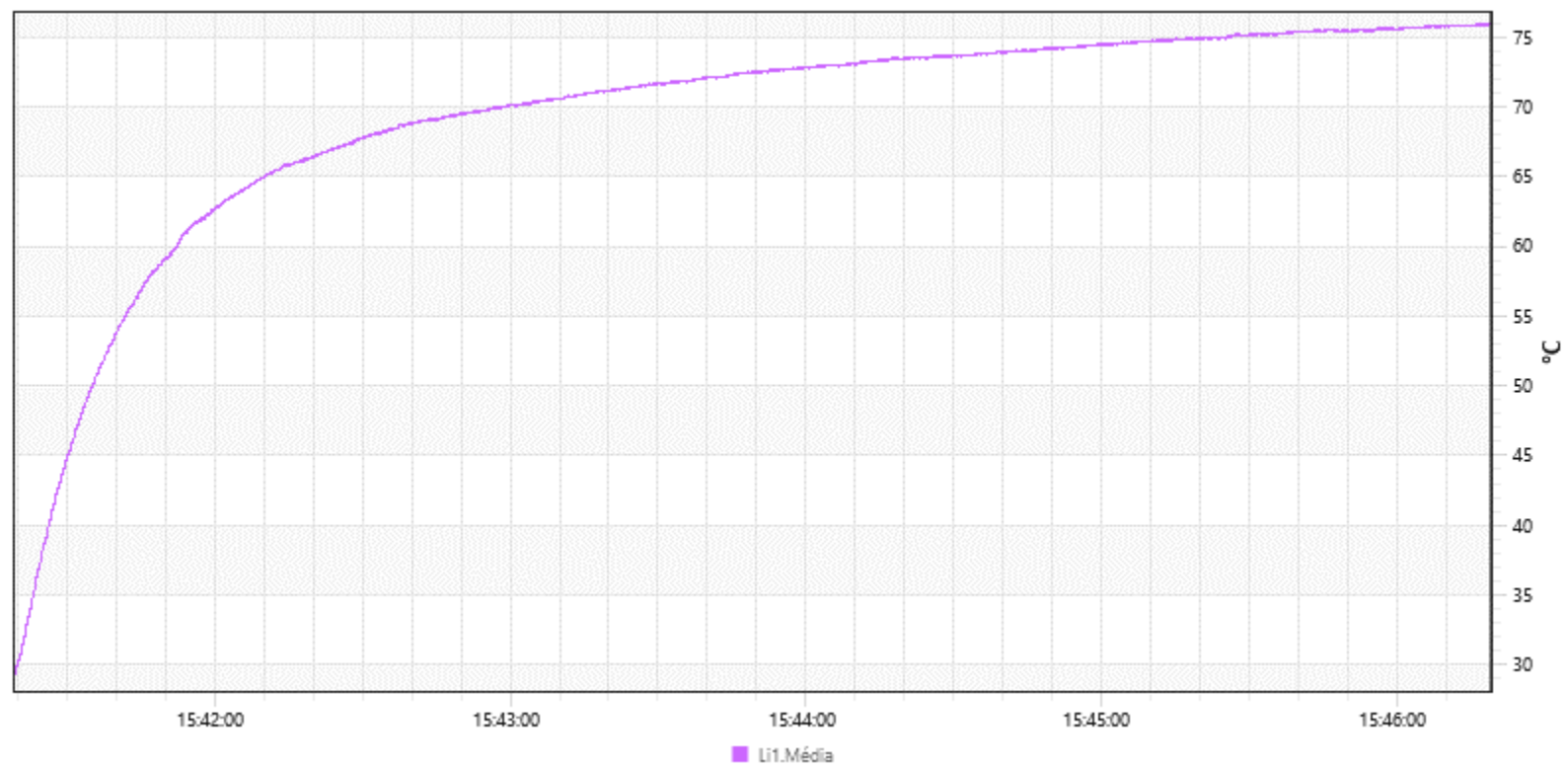
Bobbin	Conditions	Diameter (m)	Area (m²)	Resistance (Ohm)	Resistivity (Ohm.m)	Conductivity (S/m)	AV	SD	CV
OS_6	Bomba: 14 rpm Rolo 1: 100 m/min Rolo 2: 100 m/min Rolo 3: 100 m/min CDR: 1 DDR: 25	0,00083	0,00000054	3,50E+08	6,26E+03	1,60E-04	7,85E-05	5,81E-05	0,760
				2,30E+09	4,11E+04	2,43E-05			
				1,90E+09	3,40E+04	2,94E-05			
				1,60E+09	2,86E+04	3,50E-05			
				4,18E+08	7,47E+03	1,34E-04			
OS_7	Bomba: 18 rpm Rolo 1: 100 m/min Rolo 2: 100 m/min Rolo 3: 100 m/min CDR: 1 DDR: 20	0,00091	0,00000066	1,70E+09	3,71E+04	2,69E-05	3,08E-05	1,14E-05	0,369
				1,80E+09	3,93E+04	2,54E-05			
				9,50E+08	2,07E+04	4,82E-05			
				1,20E+09	2,62E+04	3,82E-05			
				3,02E+09	6,59E+04	1,52E-05			

2.4 Heating tests data

PBT/3%CNTs – 12 V



PBT/3%CNTs – 24 V



PBT/3%CNTs – 48 V

